Reconstruction of the Greenland Ice Sheet surface mass balance and the spatiotemporal distribution of freshwater runoff from Greenland to surrounding seas

SEBASTIAN H. MERNILD

Nansen Environmental and Remote Sensing Center, Bergen, NORWAY, Direction of Antarctic and Sub-Antarctic Programs, Universidad de Magallanes, Punta Arenas, CHILE, and Department of Environmental Sciences, Western Norway University of Applied Sciences, Sogndal, NORWAY

GLEN E. LISTON

Cooperative Institute for Research in the Atmosphere, Colorado State University, Fort Collins, Colorado, USA

ANDREW P. BECKERMAN

Department of Animal and Plant Sciences, University of Sheffield, UK

JACOB C. YDE

Department of Environmental Sciences, Western Norway University of Applied Sciences, Sogndal, NORWAY

Submitted to The Cryosphere, October 15, 2017

Resubmitted April 10, 2018

Corresponding author address:

Sebastian H. Mernild, e-mail: sebastian.mernild@nersc.no

Abstract

Knowledge about variations in runoff from Greenland to adjacent fjords and seas is important for the hydrochemistry and ocean research communities to understand the link between terrestrial and marine Arctic environments. Here, we simulate the Greenland Ice Sheet (GrIS) surface mass balance (SMB), including refreezing and retention, and runoff together with catchment-scale runoff from the entire Greenland landmass (n = 3,272 simulated catchments) throughout the 35-year period 1979–2014. SnowModel/HydroFlow is applied at 3-h intervals to resolve the diurnal cycle and at 5-km horizontal grid resolution using ERA-Interim (ERA-I) reanalysis atmospheric forcing. Variations in meteorological and surface ice and snow cover conditions influence the seasonal variability in simulated catchment runoff; variations in the GrIS internal drainage system are assumed negligible and a time-invariant digital elevation model is applied. Approximately 80 % of all catchments show increasing runoff trends over the 35 years, with on average relatively high and low catchment-scale runoff from the SW and N parts of Greenland, respectively. Outputs from an Empirical Orthogonal Function (EOF) analysis are combined with cross-correlations indicating a direct link (zero lag time) between modeled catchment-scale runoff and variations in the large-scale atmospheric circulation indices North Atlantic Oscillation (NAO) and Atlantic Multidecadal Oscillation (AMO). This suggests that natural variabilities in AMO and NAO constitute controls on catchment-scale runoff variations in Greenland.

KEYWORDS: Empirical Orthogonal Function; Greenland freshwater runoff; Greenland Ice Sheet; HydroFlow; Modeling; NASA MERRA; SnowModel; surface mass-balance

1. Introduction

The Greenland Ice Sheet (GrIS) is highly sensitive to changes in climate (e.g., Box et al. 2012; Hanna et al. 2013; Langen et al. 2015; Wilton et al. 2016; AMAP 2017). It is of scientific interest and importance because it constitutes a massive reserve of freshwater that discharges to adjacent fjords and seas (Cullather et al. 2016). Runoff from Greenland influences the sea surface temperature, salinity, stratification, marine ecology, and sea-level in a number of direct and indirect ways (e.g., Rahmstorf et al. 2005; Straneo et al. 2011; Shepherd et. al. 2012; Weijer et al. 2012; Church et al. 2013; Lenaerts et al. 2015).

The GrIS surface mass balance (SMB) and freshwater runoff have changed over the last decades and most significantly since the mid-1990s (e.g., Church et al. 2013; Wilton et al. 2016). For example, recent estimates by Wilton et al. (2016) showed a decrease in SMB from ~350 Gt yr^{-1} (early-1990s) to ~100 Gt yr^{-1} (in 2010–2012) and an increase in runoff from ~200 Gt yr^{-1} (early-1990s) to ~450 Gt yr^{-1} (in 2010 and 2012). Van den Broeke et al. (2016) showed a decrease in SMB from 398 Gt yr^{-1} (1961–1990) to 306 Gt yr^{-1} (1991–2015) and an increase in runoff from 256 Gt yr^{-1} (1961–1990) to 363 Gt yr^{-1} (1991–2015). For 2009 through 2012, the runoff has been estimated to include approximately two-third of the gross GrIS mass loss (Enderlin et al. 2014), while the net GrIS mass loss, on average, was 375 Gt yr^{-1} (2011–2014) (AMAP 2017). The contribution of GrIS mass loss to global mean sea-level was around 5 % in 1993, and more than 25 % in 2014 (Chen et al. 2017), and up to 43 % for the GrIS and peripheral glaciers and ice caps in 2010–2012 (Noël et al. 2017).

Runoff from the GrIS is an integrated response of rain, snowmelt, and glacier melt and other hydrometeorological processes (e.g., Bliss et al. 2014). Tedesco et al. (2016) estimated a

1979–2016 change in GrIS spatial surface melt extent of ~15,820 km^2 yr^{-1}, and a change in melt season duration of ~30–40 days in NE and 15–20 days along the west coast. At higher GrIS elevations, surface melt does not necessarily equal surface runoff because meltwater may be retained or refrozen in the porous near-surface snow and firn layers (Machguth et al. 2016), where the firn pore space provides potential storage for meltwater (Haper et al. 2012; van Angelen et al. 2013). Melt water percolation, refreezing, and densification processes are common in GrIS snow, firn, and multi-year firn layers – especially where semipermeable or impermeable ice layers are present (Brown et al. 2012; van As et al. 2016). Such physical mechanisms and conditions in the firn and multi-year firn layers lead, e.g., to non-linearity in meltwater retention (Brown et al. 2012).

The GrIS internal drainage system has received increased attention in recent years. This is, in part, because the summer acceleration of ice flow is controlled by supraglacial meltwater draining to the subglacial environment (Zwally et al. 2002; van de Wal et al. 2008; Shephard et al. 2009). Enhanced production of supraglacial meltwater results in more water supplied to the glacier bed, leading to reduced basal drag and accelerated basal ice motion. This process is referred to as basal lubrication, and it constitutes a potential positive feedback mechanism between climate change and sea-level rise (Hewitt 2013). At high GrIS elevations, surface meltwater primarily drains to the glacier bed via hydrofractures (van der Veen 2007), whereas meltwater is routed to the glacier bed via crevasses and moulins in the peripheral areas (Banwell et al. 2016; Everett et al. 2016; Koziol et al. 2017). Rapid drainage of large volumes of GrIS meltwater come from sudden release from supraglacial and proglacial lakes (known as a glacial lake outburst flood (GLOF) or jökulhlaup), which are particularly common in west Greenland (Selmes et al. 2011; Carrivick and Quincey 2014). The seasonal evolution of the structure and efficiency of the drainage system beneath the GrIS is indirectly assumed from our understanding of the subglacial hydraulic potential beneath Alpine glaciers. This general understanding is used to explain the observed seasonal changes in ice motion (Bartholomew et al. 2010, 2012) where few direct observations exist (Kohler et al. 2017). In fact, we know very little about spatiotemporal shifts in the configuration of the subglacial drainage network beneath the GrIS. We therefore assume that the subglacial drainage network in the natural system is dynamic and sensitive to rerouting of water flow between adjacent catchments (so-called water piracy; Chu et al. 2016), although we do not understand the details sufficiently to implement them in a runoff routing model.

We also lack high resolution information on the spatiotemporal distribution of GrIS and Greenland freshwater runoff to the fjords and seas, and the spatiotemporal distribution of solid-ice discharge (calving) from tidewater glaciers is also largely unknown, although Enderlin et al. (2014) estimated solid-ice discharge from around 180 tidewater glaciers . To address this lack of knowledge, information about the quantitative discharge (runoff and solid-ice discharge) conditions from the numerous catchments in Greenland is required. Available GrIS calving rates are insufficient to represent the calving rates from the entire Greenland and are therefore not generally included in overall Greenland freshwater estimates (Nick et al. 2009; Lenaerts et al. 2015). This is an unaddressed gap, which likely prevents us from comprehensively understanding the terrestrial freshwater discharge to the fjords and seas. This also limits the subsequent link between changes in terrestrial inputs and changes in the hydrographic and circulation conditions. This has further implications for ocean model simulations, where, for example, earlier representations of Greenland discharge boundary conditions were either non-existent or overly simplistic (e.g., Weijer et al. 2012).

Previous GrIS studies constructed a section-wise runoff distribution by dividing the ice sheet into six to eight overall defined sections (e.g., Rignot et al. 2008; Bamber et al. 2012; Rignot and Mouginot 2012; Lenaerts et al. 2015; Wilton et al. 2016). These studies illustrated an increase in runoff since 1870 for all GrIS sections, with the greatest increase in runoff since mid-1990s and in the southwestern part of the ice sheet.

Mernild and Liston (2012) reconstructed the GrIS SMB and the Greenland spatiotemporal runoff distribution from ~3,150 individually simulated catchments, at 5-km spatial, and daily temporal, resolutions covering the period from 1960 through 2010. Automatic weather stations located both on and off the GrIS were used for atmospheric forcings in Mernild and Liston (2012). The study was carried out using a full energy balance, multi-layer snowpack and snow distribution, and freshwater runoff model and a software package called SnowModel/HydroFlow (Liston and Elder 2006a; Liston and Mernild 2012). These individual catchment outlet runoff time series were analyzed to map runoff magnitudes and variabilities in time, but also emphasized trends and spatiotemporal variations, including runoff contributions from the GrIS, the land area (the tundra region) between the GrIS ice margin and the ocean, from the relatively small isolated glaciers and ice caps, and from entire Greenland. This approach is especially important when trying to understand the total runoff fraction from Greenland, including the annual and seasonal freshwater runoff variabilities within individual catchments.

Here, we improve the work by Mernild and Liston (2012) by using SnowModel/HydroFlow and by including a new digital elevation model (DEM). We also extend the time series to 2014 by using the ERA-Interim (ERA-I) reanalysis products on 3-h time step (Dee et al. 2011). The objective of this study is to simulate, map, and analyze first-order atmospheric forcings and GrIS mass balance components for Greenland. The analyzed variables include the GrIS SMB, together with GrIS surface air temperature, surface melt, precipitation, evaporation, sublimation, refreezing and retention, and surface freshwater runoff and specific runoff (runoff volume per time per unit drainage area, L s^{-1} km^{-2}; to convert to mm yr^{-1}, multiply by 31.6). The time period covers 1979–2014 (35 years), with a focus on the present day conditions 2005–2014. Further, the spatiotemporal magnitude, distribution, and trends of individual catchment-scale runoff and specific runoff from Greenland (n = 3,272; where n is the number of simulated catchments, each with an individual flow network) were simulated based on HydroFlow-generated watershed divides and flow networks for each catchment. The simulated spatiotemporal catchment-scale outlet runoff is useful as boundary conditions for fjord and ocean model simulations. We also analyzed the spatiotemporal catchment-scale outlet runoff using Empirical Orthogonal Functions (EOF). This analysis allowed us to describe simultaneously how the spatial patterns of catchment-scale outlet runoff changed over time. It also allowed us to explore via cross-correlations the relationship between the spatiotemporal patterns of runoff and large-scale atmospheric-ocean circulation indices including the North Atlantic Oscillation (NAO) and the Atlantic Multidecadal Oscillation (AMO), with particular attention to the lag-times, if any, between variations in NAO and AMO and responses in Greenland catchment-scale runoff.

2. Model description, setup, and evaluation

2.1 SnowModel

SnowModel (Liston and Elder 2006a) is established by six sub-models, where five of the models were used here to quantify spatiotemporal variations in atmospheric forcing, surface snow properties, GrIS SMB, and Greenland catchment runoff. The sub-model *MicroMet* (Liston and Elder 2006b; Mernild et al. 2006a) downscaled and distributed the spatiotemporal atmospheric fields using the Barnes objective interpolation scheme. Interpolation fields were adjusted using known meteorological algorithms, e.g., temperature-elevation, wind-topography, humidity-cloudiness, and radiation-cloud-topography relationships (Liston and Elder 2006b). *Enbal* (Liston 1995; Liston et al. 1999) simulated a full surface energy balance considering the influence of cloud cover, sun angle, topographic slope, and aspect on incoming solar radiation, and moisture exchanges, e.g., multilayer heat- and mass-transfer processes within the snow (Liston and Mernild 2012). *SnowTran-3D* (Liston and Sturm 1998, 2002; Liston et al. 2007) accounted for the snow (re)distribution by wind. *SnowPack-ML* (Liston and Mernild 2012) simulated multilayer snow depths, temperatures, and density evolutions. *HydroFlow* (Liston and Mernild 2012) simulated watershed divides, routing network, flow residence-time, and runoff routing (configurations based on the gridded topography), and discharge hydrographs for each grid cell including catchment outlets. These sub-models have been evaluated against independent observations with success in Greenland, Arctic, high mountain regions, and on the Antarctic Ice Sheet with acceptable results (e.g., Hiemstra et al. 2006; Liston and Hiemstra 2011; Beamer et al. 2016). For detailed information regarding the use of SnowModel for the GrIS or local Greenlandic glaciers SMB and runoff simulations, we refer to Mernild and Liston (2010, 2012) and Mernild et al. (2010a, 2014).

2.2 Meteorological forcing, model configuration and model limitations

SnowModel was forced with ERA-Interim (ERA-I) reanalysis products on a 0.75° longitude × 0.75° latitude grid from the European Centre for Medium-Range Weather Forecasts (ECMWF; Dee et al. 2011). The simulations were conducted from 1 September 1979 through 31

August 2014 (35 years) (henceforth 1979–2014), where the 6-hour (precipitation at 12-hour) temporal resolution ERA-I data was downscaled to 3-hourly values on a 5-km grid using MicroMet. The 6-hour data were scaled to 3-hours by linear interpolation, and the 12-hour precipitation was equally distributed over the 3-hour intervals for the last 12 hours. The 3-hour temporal resolution was chosen to allow SnowModel to resolve the solar radiation diurnal cycle in its simulation of snow and ice temperature evolution and melt processes.

The DEM was obtained from Levinsen et al. (2015) (original resolution 2 × 2 km; 4 km^2), and rescaled to a 5-km horizontal grid resolution that covered the GrIS (1,646,175 km^2), mountain glaciers, and the entire Greenland (2,166,725 km^2) and the surrounding fjords and seas (Figure 1a). The DEM is time-invariant specific to the year 2010. The DEM was developed by merging contemporary radar and laser altimetry data, where radar data were acquired with Envisat and CryoSat-2, and laser data with the Ice, Cloud, and land Elevation Satellite (ICESat), the Airborne Topographic Mapper (ATM), and the Land, Vegetation, and Ice Sensor (LVIS). Radar data were corrected for horizontal, slope-induced, and vertical errors from penetration of the echoes into the subsurface (Levinsen et al. 2015). Since laser data are not subject to such errors, merging radar and laser data yields a DEM that resolves both surface depressions and topographic features at higher altitudes (Levinsen et al. 2015). The distribution of glacier cover was obtained from the Randolph Glacier Inventory (RGI, v. 5.0) polygons; these data were resampled to the 5-km grid. The SnowModel land-cover mask defined glaciers to be present when individual grid cells were covered by 50 % or more with glacier ice.

In MicroMet, only one-way atmospheric coupling was provided, where the meteorological conditions were prescribed at each time step. In the natural system, the atmospheric conditions would be adjusted in response to changes in surface conditions and properties (Liston and Hiemstra 2011). Due to the use of the 5-km horizontal grid increments, snow transport and blowing-snow sublimation processes (usually produced by SnowTran-3D in SnowModel) were excluded from the simulations because blowing snow does not typically move completely across 5-km distances (Liston and Sturm 2002; Mernild et al. 2017). Static sublimation was, however, included in the model integrations. In HydroFlow, the generated catchment divides and flow network were controlled by the DEM, i.e., exclusively by the surface topography and not by the development of the glacial drainage system. The role of GrIS bedrock topography on controlling the potentiometric surface and the associated meltwater flow direction was assumed to be a secondary control on discharge processes (Cuffey and Paterson 2010).

First, the GrIS DEM was initially divided into six major sections following Rignot et al. (unpublished): southwest (SW), west (W), northwest (NW), north (N), northeast (NE), and southwest (SW) (Figure 1b and Table 1). Second, HydroFlow divided Greenland into 3,272 individual catchments (Figure 1c), each with an eight-compass-direction water-flow network where water is transported through this network via linear reservoirs. Only a single outlet into the seas was allowed for each individual catchment.

The mean and median catchment sizes were 680 km^2 and 75 km^2, respectively. The top one percent of the largest catchments accounted for 53 % of the Greenland area. This distribution of HydroFlow-defined GrIS catchments (Figure 1c) closely matched both the catchment distribution by Mernild and Liston (2012) and by Rignot and Kanagaratnam (2006) for the 20 largest GrIS catchments (not including midsize and minor catchments), both with respect to size and location of the watershed divide. The total number of HydroFlow-generated catchments presented in this study was ~4 % higher due to the use of the DEM obtained from Levinsen et al. (2015), than the number of Greenland catchments in the Mernild and Liston (2012) study.

An example of the HydroFlow generated catchment divides and flow network is illustrated in detail by Mernild et al. (2018; Figure 1c) for the Kangerlussuaq catchment in central west Greenland (67°N, 50°W; SW sector of the GrIS): The same catchment from where SnowModel/HydroFlow was evaluated against independent observations (see Section 2.3). Because the DEM is time-invariant, no changes from a thinning ice, ice retreat, and from changes in hypsometry will influence the catchment divides and the flow network patterns, including the glacial drainage system. Changes in runoff over time are therefore solely influenced by the climate signal and the surface snow and ice cover conditions (runoff was generated from gridded inputs from rain, snowmelt, and ice melt). In HydroFlow, the meltwater flow velocities were obtained from dye tracer experiments conducted both through the snowpack (in early and late-summer) and through the englacial and subglacial environments (Mernild et al. 2006b).

2.3 Evaluation

For Greenland, long-term catchment river runoff observations are sparse; at present at least eight permanent hydrometric monitoring stations are operating (Mernild 2016), measuring the sub-daily and sub-seasonal runoff variability originating from rain, melting snow, and melting ice from local glaciers and the GrIS. In addition, these observations only span parts of the runoff season, ranging between few weeks to approximately three months. For the Kangerlussuaq area, independent meteorological, snow and ice observational, and river runoff datasets are also available, e.g., K-transect point observed air temperature, and SMB and catchment outlet observed runoff (discharge) from Watson River (e.g., van de Wal et al. 2005; van den Broeke et al. 2008a; 2008b, Hasholt et. al. 2013, van As et al. 2018). These observed datasets were used for evaluation of the SnowModel/HydroFlow ERA-I simulated GrIS mean annual air temperature (MAAT), SMB, ELA (equilibrium-line altitude: the spatially averaged elevation of the equilibrium line, defined as the set of points on the glacier surface where the net mass balance is zero), and catchment river outlet freshwater runoff presented herein (Mernild et al. 2018). These model evaluations showed acceptable results for the Kangerlussuaq area, illustrating a difference between observations and simulations, for example, in MAAT of 0.2–0.5°C (1993–2014) and in GrIS SMB of 0.17 ± 0.23 m w.e. (1990–2014), where the r^2-value (r^2 is the explained variance) ranged between 0.55 and 0.67 (linear), except for one AWS in the K-Transect where r^2 was 0.28 (AWS S6). The simulated Kangerlussuaq mean GrIS ELA (1979–2014) was located at 1,760 ± 260 m a.s.l. In van As et al. (2018), the ELA was defined as the altitude where SMB minus refreezing equals zero, and it was located at approximately 1,800 m a.s.l. (2009–2015), and in van de Wal et al. (2012) ELA was estimated to approximately 1,610 m a.s.l. (1991–2014) (Mernild et al. 2018). Simulated Kangerlussuaq catchment river outlet runoff was, however, on average overestimated by 31 ± 9 % (2007–2013) and subsequently adjusted against observed runoff (r^2 = 0.76 (linear); for further information see Mernild et al. 2018). This freshwater runoff overestimation is likely related to the missing multiyear firn processes in SnowModel, such as nonlinear meltwater retention, percolation blocked by ice layers, and refreezing. Due to the limited long-term river runoff observations from the GrIS, the Kangerlussuaq runoff adjustment from Mernild et al. (2018) was used herein for the entire GrIS. The adjusted GrIS runoff is henceforth referred to as runoff.

Further, the use of ERA-I has also showed promising results after a full evaluation estimating changes in ice sheet SMB for the catchments linked to Godthåbsfjord (64° N) in Southwest Greenland (Langen et al. 2015).

In the analysis that follows, all correlation trends declared 'significant' are statistically significant at or above the 5 % level ($p<0.05$; based on a linear regression t test).

2.4 Surface water balance components

For the GrIS, surface water balance components can be estimated using the hydrological method (continuity equation) (Equation 1):

$$P - (Su + E) - R + \Delta S = 0 \pm \eta, \qquad (1)$$

where P is precipitation input from snow and rain, Su is sublimation from a static surface, E is evaporation, R is runoff from snowmelt, ice melt, and rain, ΔS is change in storage (ΔS is also referred to as SMB) derived as the residual value from changes in glacier and snowpack storage. For snow and ice surfaces, the ablation was estimated as: $Su + E + R$. The amount of snow refreezing and retention was estimated as: $P_{rain} + melt_{surface} - R$ (for bare ice: $P_{rain} + melt_{surface} = R$). The parameter η is the water balance discrepancy. This discrepancy should be 0 (or small), if the components P, Su, E, R, and ΔS have been determined accurately.

3. EOF runoff analysis

We applied an Empirical Orthogonal Function (EOF) analysis to define the spatiotemporal pattern in simulated catchment outlet runoff. EOF is a statistical tool that analyzes spatial and temporal runoff data to find combinations of locations that vary consistently through time, and combinations of time, that vary in a spatially consistent manner (e.g., Preisendorfer 1998; Sparnocchia et al. 2003). The major axes of the EOF analysis identify variations in the catchment outlet runoff in both time and space.

The eigenvalues of the EOFs can be correlated with the temporal data, and the eigenvectors with spatial locations, to identify how the EOF describes change in runoff in time and across space. Furthermore, the temporal patterns embedded in the EOFs can, via cross-correlation analysis, be related to larger scale atmospheric-ocean indices (Mernild et al. 2015), in this case the North Atlantic Oscillation (NAO) and Atlantic Multi-decadal Oscillation (AMO). The NAO and AMO indices were obtained from Hurrell and van Loon (1997) and Kaplan et al. (1998), respectively. The latter analysis enables to link fluctuations in , for example, NAO or AMO to GrIS catchment mass-loss and outlet river runoff (the lag in the cross-correlation analyses tells us these details).

We focused on the NAO and AMO for several reasons. NAO is estimated based on the mean sea-level pressure difference between the Azores High and Icelandic Low. NAO is a large-scale atmospheric circulation index, and is therefore a good measure of airflow and jet-stream moisture transport variability (e.g., Overland et al. 2012) from the North Atlantic onto Northwest Europe (Dickson et al. 2000; Rogers et al. 2001). According to Hurrell (1995), a positive NAO is associated with cold conditions in Greenland, while a negative NAO corresponds to mild conditions. AMO is a large-scale oceanic circulation index, and an expression of fluctuating mean sea-surface temperatures in the North Atlantic (Kaplan et al. 1998). For example, Arctic land surface air temperatures are highly correlated with the AMO (Chylek et al. 2010), and the overall annual trend in the mean GrIS melt extent correlates with the smoothed trends of the AMO (Mernild et al. 2011). A positive AMO indicates relatively high surface air temperature and less precipitation at high latitudes (relatively high net mass loss), whereas a negative AMO indicates relatively low surface air temperature and a higher precipitation (relatively low net mass balance loss) (Kaplan et al. 1998).

4. Results and discussion

4.1 GrIS surface water balance conditions

Figure 2 presents the SnowModel ERA-I simulated 35-year mean spatial GrIS surface MAAT, precipitation, surface melt, evaporation and sublimation, ablation, and SMB. Overall, all variables follow the expected spatial patterns. For example, the lowest MAAT occurred at the GrIS interior (≤ -27°C) and highest values were at the margin (≥ 0°C). Also, the lowest annual mean precipitation values were situated in the northern half of the GrIS interior (≤ 0.25 m water equivalent (w.e.)), while peak values occurred in the southeastern part of Greenland (≥ 3.5 m w.e.). The lowest annual mean surface melt values (≤ 0.0625 m w.e.) were present at the upper parts of the GrIS and vice versa at the lowest margin areas (≥ 5.0 m w.e.). The 35-year mean SMB illustrated net loss at the lowest elevations of ≥ 3.5 m w.e. and net gain at the highest elevations of between 0 and 0.25 m w.e. The peak net gain of ≥ 3.0 m w.e. occurred in Southeast Greenland, which matches what is generally expected from the overall precipitation pattern over the GrIS. The SnowModel ERA-I spatial simulated 35-year mean distributions generally agree with previous studies by Fettweis et al. (2008, 2017), Hanna et al. (2011), and Box (2013), within the different temporal domains covered by these studies.

On GrIS section-scale (Table 1), a clear variability between the six sections (Figure 1b) occurred for the surface mass-balance components (Equation 1) for both the 35-year mean and the last decade. On average, most precipitation fell in the Southeast Greenland sector of 242.6 ± 39.1 Gt yr^{-1} (where, ± equals one standard deviation). This was likely due to the cyclonicity between Iceland and Greenland, which typically sets up a prevailing easterly airflow towards the steep slopes of the southern coast of Greenland, generating orographic enhancement (Hanna et al. 2006; Bales et al. 2009). The lowest 35-year mean precipitation of 31.1 ± 5.4 Gt yr^{-1} occurred in the dry North Greenland. For the last decade, the mean annual precipitation was 232.4 ± 25.2 Gt yr^{-1} and 30.9 ± 5.1 Gt yr^{-1} for Southeast Greenland and North Greenland, respectively. This regional distribution is in accordance with the study on Greenlandic precipitation patterns by Mernild et al. (2015), although their analysis was based on observed precipitation from 2001–2012. Further, in Mernild et al. (2018; Figure 6b), the mean ERA-I grid point precipitation (located closest to the center of the Kangerlussuaq watershed) was tested against Kangerlussuaq SnowModel ERA-I downscaled mean catchment precipitation conditions; this analysis indicated no significant difference between the two datasets.

The ratio between rain and snow precipitation varied from <1 % (Northeast section) to 5 % (Southwest section), averaging 2 % and indicating that rain only played a minor role in the GrIS precipitation budget (Table 1). For the last decade, the average rainfall-to-snowfall ratio was 3 % for the entire GrIS.

For the GrIS, the overall precipitation was 653.9 ± 66.4 Gt yr^{-1} (35 years) and 645.0 ± 39.0 Gt yr^{-1} (2005–2014), which is within the lower range of previously reported values (Fettweis et al. 2017; Table 1). For example, in MAR (Modèle Atmosphérique Régional; v. 3.5.2) the simulated precipitation was between 642.0 and–747.0 Gt yr^{-1} (1980–1999; snowfall plus rainfall) forced with a variety of forcings, e.g., ERA-40 (Uppala et al. 2005), ERA-I (Dee et al. 2011), JRA-55 (Japanese 55-year Reanalysis; Kobayashi et al. 2015).

As shown by Fettweis et al. (2017), precipitation is the parameter with the largest uncertainty due to the spread among the different forcing datasets. Also, systematic observational errors may occur during precipitation monitoring, such as wind-induced undercatch, because of turbulence and wind field deformation from the precipitation gauge, wetting losses, and trace amounts (e.g., Goodison et al. 1989; Metcalfe et al. 1994; Yang et al. 1999; Rasmussen et al. 2012). This highlights the importance of accurately representing precipitation for estimating the energy and moisture balances, surface albedo, GrIS SMB conditions, and, in a broader perspective, the GrIS´s contribution to sea-level changes.

Besides precipitation, melt (including extent, intensity, and duration) and ablation are other relevant parameters for estimation and understanding GrIS SMB. Surface melt can influence albedo, as wet snow absorbs up to three times more incident solar energy than dry snow (Steffen 1995), and the energy and moisture balances. Changes in the amount of meltwater also affect total runoff, but also ice dynamics, and subglacial lubrication and sliding processes (Hewitt 2013).

Surface melt varied on a section-scale, for the 35-year mean, from 57.2 ± 24.1 Gt yr^{-1} in North Greenland to 155.2 ± 48.4 Gt yr^{-1} in Southwest Greenland (Table 1). The average for the entire GrIS was 542.9 ± 175.3 Gt yr^{-1} (Table 1). During the last decade, the surface melt for the GrIS had increased to 713.4 ± 138.6 Gt yr^{-1}, varying from 75.9 ± 26.9 Gt yr^{-1} in the north of Greenland to 202.4 ± 39.2 Gt yr^{-1} in Southwest Greenland. This is an increase of 31 % for the last decade compared to the entire simulation period, which was likely due to increasing MAAT (assuming an empirical relationship between air temperature (sensible heat) and surface melt rates) throughout the simulation period (Hanna et al. 2012).

The GrIS ablation patterns varied as expected between the northern and southwestern sections from 50.2 ± 15.6 Gt yr^{-1} in the north to 98.1 ± 29.2 Gt yr^{-1} in the southwest. For the entire GrIS, the mean annual ablation was 400.9 ± 106.2 Gt yr^{-1} and 510.0 ± 81.7 Gt yr^{-1} for the

35-year period and 2005–2014, respectively. This was equal to an increase of 28 %, which was also reflected in the differences in variability from 62.3 ± 17.0 Gt yr^{-1} in North Greenland to 127.3 ± 23.9 Gt yr^{-1} in Southwest Greenland (Table 1).

Runoff is a part of the ablation budget and therefore must be quantified to understand GrIS mass balance changes. Runoff varied from 34.5 ± 15.7 Gt yr^{-1} in North Greenland to 77.7 ± 28.9 Gt yr^{-1} in Southwest Greenland, averaging 288.7 ± 104.3 Gt yr^{-1} for the 35-year mean period over the GrIS. For 2005–2014, the mean runoff was 395.4 ± 82.7 Gt yr^{-1}; a 37 % increase (Table 1). For the period 1991–2015 van den Broeke et al. (2016) estimated on average the GrIS runoff to 363 ± 102 Gt yr^{-1}. The increase in SnowModel simulated GrIS runoff over time confirms the results from previous studies (e.g., van den Broeke et al. 2016, Wilton et al. 2016). On a regional-scale, runoff varied from 46.6 ± 17.3 Gt yr^{-1} in North Greenland to 106.6 ± 25.0 Gt yr^{-1} in Southwest Greenland. The simulated section runoff distribution was largely in agreement with trends noted by Lewis and Smith (2009) and Mernild and Liston (2012). The section runoff variability roughly followed the precipitation patterns, where sections with high precipitation equaled low runoff (e.g., in Southeast Greenland) and vice versa (e.g., in Southwest Greenland). More specifically, GrIS snowpack retention and refreezing processes suggest that sections with relatively high surface runoff were synchronous with relatively low end-of-winter snow accumulation because more meltwater was retained in the thicker, colder snowpack, reducing and delaying runoff to the internal glacier drainage system (e.g., Hanna et al. 2008). However, in maritime regions such as Southeast Greenland, high surface runoff can result from abnormally wet conditions (Mernild et al. 2014). Furthermore, runoff was negatively correlated to surface albedo and snow cold content, as confirmed by Hanna et al. (2008) and Ettema et al. (2009).

For the dry North and Northeast Greenland (Table 1), the relatively low end-of-winter snowpack melted relatively fast during spring warm-up. After the winter snowpack had ablated, the ice surface albedo promoted a stronger radiation-driven ablation and surface runoff, owing to the lower ice albedo. For the wetter Southeast Greenland (Table 1), the relatively high end-of-winter snow accumulation, combined with frequent summer snow precipitation events, kept the albedo high. Therefore, in that region the snowpack persists longer compared to the drier parts of the GrIS before ablation started to affect the underlying glacier ice.

Regarding specific runoff (runoff volume per unit drainage area per time, L s^{-1} km^{-2}; to convert to mm yr^{-1}, multiply by 31.6), maximum values of 11.5 L s^{-1} km^{-2} and 15.8 L s^{-1} km^{-2} were seen in Southwest Greenland for the mean 35-year and 2005–2014 periods, respectively. The minimum values of 3.0 L s^{-1} km^{-2} and 4.3 L s^{-1} km^{-2} for the mean 35-year and 2005–2014 periods, respectively, occurred in Northeast Greenland (Table 2). On average for the GrIS, the corresponding specific runoffs were 5.6 L s^{-1} km^{-2} and 7.6 L s^{-1} km^{-2}, respectively, which are within the range of our previous study (e.g., Mernild et al. 2008). Specific runoff is a valuable tool for comparing runoff on regional and catchment scales, where regions and catchments vary in size.

Refreezing and retention in the snow and firn packs were defined as rain plus surface melt minus runoff (see Section 2.4). For the GrIS, the 35-year mean refreezing and retention was estimated to be 49 % (269.9 ± 77.4 Gt yr^{-1}), and it was 45 % (318.0 ± 62.8 Gt yr^{-1}) for 2005–2014 (Table 1). Hence, refreezing and retention provided an important quantitative contribution to the evolution of snow and firn layers, ice densities, snow temperatures (cold content or snow temperatures below freezing), and moisture available for runoff (Liston and Mernild 2012). The SnowModel ERA-I refreezing and retention simulations were within the order of magnitude (~45

%) produced by byNoël et al. (2017) and Steger et al. (2017), where Steger et al. (2017) showed values in the range between 216–242 Gt yr^{-1} (1960–2014). . Vizcaino et al. (2013), however, indicated refreezing values representing 35% of the available liquid water (the sum of rain and melt). On the regional-scale for the GrIS, the 35-year mean refreezing and retention value varied from 40 % in North Greenland to 57 % in Southwest Greenland. For 2005–2014, the values were 39 % for North Greenland and 57 % for Southeast Greenland (Table 1), indicating a clear variability in refreezing and retention between the different regions.

In Figure 3a, the time series of GrIS mean annual refreezing and retention shows an increasing trend (significant) and variability ranging from 0.07 m w.e. (1992) to 0.29 m w.e. (2012), with an annual mean value of 0.16 ± 0.04 m w.e. In Figure 3b, the spatial 35-year mean GrIS refreezing and retention is presented together with values from 1992 and 2012, the minimum and maximum years, respectively. The mean spatial distribution highlights minimal refreezing and retention at the GrIS interior, whereas areas with low elevation had values above 0.75 m w.e. in southern part of the GrIS. For the minimum year 1992, the pattern was more pronounced with no refreezing and retention in the interior. The maximum year 2012 on the other hand had refreezing and retention at the interior (between 0 and 0.025 m w.e.) (Figure 3b). This was likely due to the extreme GrIS surface melt event throughout July 2012 (e.g., Nghiem et al. 2012; Hanna et al. 2014). When divided into regions and catchments, the 2012 simulated refreezing and retention showed a clear separation between highest values in Southwest Greenland and lowest values in Northeast and East Greenland. Because here, refreezing and retention were estimated as the sum of rain and melt minus the sum of runoff, this SnowModel analysis did not provide a detailed description of the physical mechanisms and conditions (beyond the standard SnowModel snowpack temperature and density evolution) leading to, e.g., non-linearities in snow and firn meltwater retention (Brown et al. 2012). A model that does not include refreezing and retention processes in its snow and firn evolution calculations, and the associated impacts on SMB, will introduce additional uncertainty in it calculations of GrIS SMB and its contribution to sea-level change.

The GrIS SMB for the 35-year mean was 253.4 ± 121.4 Gt yr^{-1}, indicating a negative sea-level contribution, and 135.5 ± 98.2 Gt yr^{-1} for 2005–2014, indicating a trend towards a less positive SMB value (Table 1). This change in SMB between the two periods was mainly due to an increase in runoff of 106.7 Gt yr^{-1}, where other water balance components showed relatively lesser increases. For comparison e.g., Vizcaino et al. (2013), Noël et al. (2016), and Wilton et al. (2016) estimated the mean GrIS SMB to be 359.3 ± 120 Gt yr^{-1} (1960–2005), 349.3 Gt yr^{-1} (1958–2015), and 382 ± 78 Gt yr^{-1} (1979–2012), respectively. For the GrIS, the 35-year mean SMB was negative for the northern region, in balance for northeast Greenland, and positive for all other regions and only positive for the southeastern, southwestern, and western sectors for 2005–2014 (Table 1).

The linear trends for the different water balance components are shown in Table 1. For the 35-year period, significant trends occurred for rain, surface melt, runoff, ablation, refreezing and retention, and SMB (highlighted in bold in Table 1), where all except SMB showed positive trends (note that SMB loss is calculated as negative by convention). In Figure 4, selected GrIS parameters are illustrated, where, for example, SMB showed a negative trend of -66.2 Gt decade^{-1} (significant), heading towards a less positive balance at the end of the simulation period (Figure 4). For 2005–2014, however, the SMB trend was positive 16.6 Gt decade^{-1} (insignificant). Similar positive SMB trends have previously been shown in studies by Hanna et al. (2011), Tedesco et al. (2014), Fettweis et al., (2008, 2011, 2013) and Wilton et al. (2016), even though variabilities in mean SMB occur between the different studies. Wilton et al. (2016) estimated the GrIS SMB to be ~~150 Gt yr^{-1} for 2002–2012 and ~100 Gt for the years 2010–2012. Further, for 2005–2014, air temperature, precipitation, surface melt, sublimation and evaporation, and runoff trends were all negative (insignificant) (Figure 4 and Table 1).

4.2 Greenland spatiotemporal runoff distribution and EOF analysis

The Greenland 35-year simulated catchment outlet runoff and specific runoff distribution are shown in Figure 5. Each circle represents the volume (individual catchment outlet hydrographs are not shown), including runoff from thousands of glaciers located between the GrIS margin and the surrounding seas. The 35-year mean catchment outlet runoff varied from <0.0001 to ~20 × 10^9 m^3 (Figure 5a) and specific runoff from <0.1 to ~90 L s^{-1} km^{-2} (Figure 5b). Catchment runoff variability depends on the regional climate conditions, land-ice area cover, elevation range (including hypsometry) within each catchment, and catchment area. Here the length in runoff season varied from two to three weeks in the north to four to six months in the south. The median annual catchment runoff and specific runoff were 0.018 × 10^9 m^3 and 6.4 L s^{-1} km^{-2}, respectively. The median specific runoff value is in agreement with previous studies (e.g., Mernild et al. 2010a). Further, the variance in catchment runoff and specific runoff varied from <0.0001 to 7.1 × 10^9 m^3 and <0.01 to 15.3 L s^{-1} km^{-2}, respectively, with a median variance of 0.004 × 10^9 m^3 and 1.8 L s^{-1} km^{-2} (Figures 5a and 5b). Regarding the linear trend in annual runoff, both increasing and decreasing trends occurred over the 35 years. In total, 81 % (19 %) of all catchments had increasing (decreasing) runoff trends over the 35 years (all of the decreasing trends were insignificant). For western Greenland catchments, only increasing runoff trends occurred (Figures 5a and 5b). The runoff and specific runoff trends varied among catchments from -0.06 to 3.8 × 10^9 m^3 $decade^{-1}$ and from -0.9 to 9.0 L s^{-1} km^{-2} $decade^{-1}$, respectively, with a median value of <0.001 × 10^9 m^3 and 0.4 L s^{-1} km^{-2} $decade^{-1}$ (Figures 5a and 5b).

The EOF analysis of runoff returned three axes that captured 26, 18 and 14 % of the variance in runoff from the simulated SnowModel ERA-I annual catchment runoff (Figure 6a and S1). Following several significance tests, only EOF1 captured significant variation. In Figure 6a, the temporal pattern in EOF1, with a 5-year running mean, reveals a pattern of positive running mean values for the first two decades of the simulation period (1979–1999), and negative values hereafter (2000–2014). When EOF1 is positive, Greenland runoff is relatively low and vice versa (Figure 6b). Overall, this indicates a positive temporal trend in runoff; as EOF1 decreases, runoff increases. While not significant based on EOF test metrics, EOF2 and EOF3 patterns are less pronounced and in anti-phase to each other (Figure S1).

The temporal cycle of EOF patterns has associated spatial elements, derived from the eigenvectors (Figure 6c and S2). The eigenvectors in Figures 6c and S2 reveal the spatial pattern as a correlation between temporal trends captured by the EOFs and each individual Greenland catchment. These data indicate that the temporal trend of increasing runoff captured in EOF1 is shared by nearly all catchments in Greenland (Figure 6c). Because decreasing EOF1 values indicate increasing runoff, a negative correlation with EOF1 in space indicates increasing runoff. Catchment numbers greater than #2500 (Figure 6c) are located in Southeast Greenland and are in contrast to this. These catchments (~20 % of the catchments in Southeast Greenland) experience a distinct out-of-phase pattern of runoff compared to the Southeast Greenland runoff and the overall Greenland conditions for the last 35 years.

This difference between Southeast Greenland and the rest of Greenland supports previous findings (e.g., Lenaerts et al. 2015) proposing that variabilities in runoff are not only influenced by melt conditions, but also by precipitation patterns (primarily the end-of-winter snow accumulation), where high precipitation equals low runoff conditions such as in Southeast Greenland. Furthermore, patterns were also detected to be associated to EOF2 and EOF3 (Figure S2). These EOF2 and EOF3 patterns differed from EOF1, and they were associated with a different geographic breakdown, where both positive and negative correlations were seen for all regions. The physical mechanism behind these distributions is not clear.

There were correlations between the EOF1 and regional climate patterns expressed by the AMO and NAO (Figure 7). We found a negative correlation between EOF1 and AMO (r = 0.68; significant, p<0.01), suggesting that stronger AMO is associated with lower EOF1 values which are indicative of higher runoff (Figure 7a). In contrast, we found a positive correlation between EOF1 and NAO (r = 0.40; significant, p<0.01), suggesting that NAO values are associated with higher EOF1 values which are indicative of lower runoff (Figure 7b). For AMO, the lags are centered near zero, suggesting an immediate, real time correlation between AMO and runoff. In contrast, the strongest lag in the NAO-EOF1 relationships is at -2, suggesting a short delay in effects. Lags of 0 and -2 are not large, indicating that overall, large-scale natural variability in AMO and NAO are associated in time to catchment runoff variations in Greenland.

Mernild et al. (2011) emphasized that trends in AMO (smoothed) was analogous to trends in GrIS melt extent, where increasing AMO equaled increasing melt extent, and vice versa. Further, Chylek et al. (2010) showed that the Arctic detrended temperatures were highly correlated with AMO. However, this issue requires further investigation to establish the details of, and the mechanisms behind, the interrelationships.

5. Conclusions

Greenland catchment outlet runoff is rarely observed and studied, although quantification of runoff from Greenland is crucial for our understanding of the link between a changing climate and changes in the cryosphere, hydrosphere, and atmosphere. We have reconstructed the impact of changes in climate conditions on hydrological processes at the surface of the GrIS for the 35-year period 1979–2014. We have also simulated the Greenland spatiotemporal distribution of refreezing and retention, and freshwater runoff to surrounding seas by merging SnowModel (a spatially distributed meteorological, full surface energy balance, snow and ice evolution model) with HydroFlow (a linear-reservoir run-off routing model) forced by ERA-I atmospheric forcing data. Before simulating the individual catchment runoff to downstream areas, the catchment divides and flow networks were estimated, yielding a total of 3,272 catchments in Greenland.

For the GrIS, the simulated spatial distribution and time series of surface hydrological processes were in accordance with previous studies, although precipitation and SMB were in the lower range of these studies. Overall, Greenland has warmed and the runoff from Greenland has increased in magnitude. Specifically, 81 % of the catchments showed increasing runoff trends over the simulation period, with relatively high and low mean catchment runoff from the southwestern and northern parts of Greenland, respectively. This indicates distinct regional-scale runoff variability in Greenland. Runoff variability with near zero lag time suggests a real-time covariation between the pattern in EOF1 and changes in AMO and NAO. This suggests that runoff variations are related to large-scale natural variability of AMO and NAO in Greenland. The physical mechanism behind this phenomenon is unclear, unless it is a response to "long-term" cycles in AMO and NAO.

The simulated runoff can be used as boundary conditions in ocean models to understand hydrologic links between terrestrial and marine environments in the Arctic. Changes and variability in runoff from Greenland are expected to play an essential role in the hydrographic and circulation conditions in fjords and the surrounding ocean under a changing climate.

Acknowledgements

We thank the Nansen Environmental and Remote Sensing Center (NERSC) and Japan Society for the Promotion of Science (JSPS) for financial support under project number S17096, and the Western Norway University of Applied Sciences (HVL) for travel funds. All model data requests should be addressed to the first author. The authors have no conflict of interest.

References

AMAP, 2017. Snow, Water, Ice and Permafrost. Summary for Policy-makers. Arctic Monitoring and Assessment Programme (AMAP), Oslo, Norway, 20 pp.

Bales, R. C., Guo, Q., Shen, D., McConnell, J. R., Du, G., Burkhart, J. F., Spikes, V. B., Hanna, E., and Cappelen, J. 2009. Annual accumulation for Greenland updated using ice core data developed during 2000–2006 and analysis, of daily coastal meteorological data. J. Geophys. Res., 114, D06116, doi:10.1029/2008JD011208.

Bamber, J., van den Broeke, M., Ettema, J., Lenaerts, J., and Rignot, E., 2012. Recent large increases in freshwater fluxes from Greenland into the North Atlantic. *Geophys. Res. Letts.*, 39, L19501, doi:10.1029/2012GL052552.

Banwell, A., Hewitt, I., Willis, I., and Arnold, N. 2016. Moulin density controls drainage development beneath the Greenland ice sheet. J. Geophys. Res. Earth Surf., 121, 2248–2269.

Bartholomew, I., Nienow, P., Mair, D., Hubbard, A., King, M. A., and Sole, A. 2010. Seasonal evolution of subglacial drainage and acceleration in a Greenland outlet glacier. Nat. Geosci., 3(6), 408–411.

Bartholomew, I., Nienow, P., Sole, A., Mair, D., Cowton, T., and King, M. 2012. Short-term variability in Greenland ice sheet motion forces by time-varying meltwater drainage: Implications for the relationship between subglacial drainage system behavior and ice velocity. J. Geophys. Res., 117, F03002, doi:10.1029/2011JF002220.

Beamer, J. P., Hill, D. F., Arendt, A., and Liston, G. E. 2016. High-resolution modeling of coastal freshwater discharge and glacier mass balance in the Gulf of Alaska watershed. Water Resour. Res., 52, 3888–3909, doi:10.1002/2015WR018457.

Bliss, A., Hock, R., and Radić, V. 2014. Global response of glacier runoff to twenty-first century climate change, J. Geophys. Res. Earth Surf, 119, doi:10.1002/2013JF002931.

Box, J. E. 2013. Greenland ice sheet mass balance reconstruction, Part II: Surface mass balance (1840–2010). Journal of Climate, 26, 6974–6989, doi:10.1175/JCLI-D-12-00518.1.

Box, J. E., Cappelen, J., Chen, C., Decker, D., Fettweis, X., Mote, T., Tedesco, M., van de Wal, R. S. W., and Wahr, J. 2012. Greenland Ice Sheet. In Jeffries, M. O., Richter-Menge, J. A., and Overland, J. E. (Eds). Arctic Report Card 2012, http://www.arctic.noaa.gov/reportcard.

Brown, J., Bradford, J., Harper, J., Pfeffer, W. T., Humphrey, N., and Mosley-Thompson, E., 2012. Georadar-derived estimates of firn density in the percolation zone, western Greenland ice sheet. *Journal of Geophysical Research*, 117, F01011, doi:10.1029/2011JF002089.

Carrivick, J. L., and Quincey, D. J., 2014. Progressive increase in number and volume of ice-marginal lakes on the western margin of the Greenland Ice Sheet. *Global and Planetary Change*, 116, 156-163, doi:10.1016/j.gloplacha.2014.02.009.

Chen, X., Zhang, X., Church, J. A., Watson, C. S., King, M. A., Monselesan, D., Legresy, B., and Harig, C. 2017. The increasing rate of global mean sea-level rise during 1993–2014. Nature Climate Change, doi:10.1038/nclimate3325.

Chu, W., Creyts, T., and Bell, R. E., 2016. Rerouting of subglacial water flow between neighboring glaciers in West Greenland. J. Geophys. Res. Earth Surf., 121, 925–938.

Church, J. A., Clark, P. U., Cazenave, A., Gregory, J. M., Jevrejeva, S., Levermann, A., Merrifield, M. A., Milne, G. A., Nerem, R. S., Nunn, P. D., Payne, A. J., Pfeffer, W. T., Stammer, D., and Unnikrishnan, A. S. 2013. Sea Level Change. In: Climate Change 2013: The Physical Science Basis. Contribution of Working Group I to the Fifth Assessment Report of the Intergovernmental Panel on Climate Change [Stocker, T.F., Qin, D., Plattner, G.-K., Tignor, M., Allen, S.K., Boschung, J., Nauels, A., Xia, Y., Bex, V. and, Midgley, P.M. (eds.)]. Cambridge University Press, Cambridge, United Kingdom and New York, NY, USA.

Chylek, P., C.K. Folland, G. Lesins and M.K. Dubey. 2010. Twentieth century bipolar seesaw of the Arctic and Antarctic surface air temperatures. Geophys. Res. Lett., 37(8), L08703, doi:10.1029/2010GL042793.

Cuffey, K. M. and Paterson, W. S. B. 2010. The Physics of Glaciers. Fourth Edition. Elsevier, pp. 693.

Cullather R. I., Nowicki, S. M. J., Zhao, B., and Koenig, L. S. 2016. A Characterization of Greenland Ice Sheet Surface Melt and Runoff in Contemporary Reanalyses and a Regional Climate Model. Front. Earth Sci., 4(10), doi:10.3389/feart.2016.00010.

Dee, D. P., Uppala, S. M., Simmons, A. J., Berrisford, P., Poli, P., Kobayashi, S., Andrae, U., Balmaseda, M. A., Balsamo, G., Bauer, P., Bechtold, P., Beljaars, A. C. M., van de Berg, L., Bidlot, J., Bormann, N., Delsol, C., Dragani, R., Fuentes, M., Geer, A. J., Haimberger, L., Healy, S. B., Hersbach, H., Holm, E. V., Isaksen, L., Kållberg, P., Kohler, M., Matricardi, M., McNally, A. P., Monge-Sanz, B. M., Morcrette, J.-J., Park, B.-K., Peubey, C., de Rosnay, P., Tavolato, C., Thepaut, J.-N., Vitart, F. 2011. The ERA-Interim reanalysis: configuration and performance of the data assimilation system. Q. J. R. Meteorol. Soc., 137, 553–597, doi:10.1002/qj.828.

Dickson, R. R., Osborn, T. J., Hurrell, J. W., Meincke, J., Blindheim, J., Adlandsvik, B., Vinje, T., Alekseev, G., and Maslowski, W. 2000. The Arctic Ocean response to the North Atlantic Oscillation. Journal of Climate, 13, 2671–2696.

Enderlin, E. M., Howat, I. M., Jeong, S., Hoh, M.-J., van Angelen, J. H., and van den Broeke, M. R. 2014. An improved mass budget for the Greenland ice sheet. Geophysical Research Letters, 41(3), 866–872.

Ettema, J., van den Broeke, M. R., van Meijgaard, E., van den Berg, W. J., Bamber, J. L., Box, J. E., and Bales, R. C. 2009. Higher surface mass balance of the Greenland ice sheet revealed by high-resolution climate modeling. Geophysical Research Letters, 36, L12501.

Everett, A., Murray, T., Selmes, N., Rutt, I. C., Luckman, A., James, T. D., Clason, S., O´Leary, M., Karunarathna, H., Moloney, V., and Reeve, D. E. 2016. Annual down-glacier drainage of lakes and water-filled crevasses at Helheim Glacier, southeast Greenland. J. Geophys. Res. Earth Surf., 121, 1819–1833.

Fettweis, X., Box, J. E., Agosta, C., Amory, C., Kittel, C., Lang, C., van As, D., Machguth, H., and Gallée, H., 2017. Reconstructions of the 1900–2015 Greenland ice sheet surface mass balance using the regional climate MAR model. The Cryosphere, 11, 1015–1033, doi:10.5194/tc-11-1015-2017.

Fettweis, X., Franco, B., Tedesco, M., van Angelen, J. H., Lenaerts, J. T. M., van den Broeke, M. R., and Gallée, H., 2013. Estimating the Greenland ice sheet surface mass balance contribution to future sea level rise using the regional atmospheric climate model MAR. The Cryosphere, 7, 709 469–489.

Fettweis, X., Hanna, E., Gallée, H., Huybrechts, P., and Erpicum, M. 2008. Estimation of the Greenland ice sheet surface mass balance for the 20th and 21st centuries, The Cryosphere, 2, 117–129, doi:10.5194/tc-2-117-2008.

Fettweis, X., Tedesco, M., van den Broeke, M., and Ettema, J., 2011. Melting trends over the Greenland ice sheet (1958–2009) from spaceborne microwave data and regional climate models. The Cryosphere, 5, 359–375.

Goodison, B. E., Sevruk, B., and Klemm, S. 1989.WMO solid precipitation measurement intercomparison: objectives, methodology, analysis. IAHS publication, 179, 57–64.

Hanna, E., Fettweis, X., Mernild, S. H., Cappelen, J., Ribergaard, M., Shuman, C., Steffen, K., Wood, L., and Mote, T. 2014. Atmospheric and oceanic climate forcing of the exceptional Greenland Ice Sheet surface melt in summer 2012. *International Journal of Climatology*, 34, 1022–1037.

Hanna, E., Huybrechts, P., Cappelen, J., Steffen, K., Bales, R., Burgess, E., McConnell, J., Steffensen, J. P., Van den Broeke, M., Wake, L., Bigg, B., Griffiths, M., and Savas, D. 2011. Greenland Ice Sheet surface mass balance 1870 to 2010 based on Twentieth Century Reanalysis, and links with global climate forcing, Journal of Geophysical Research, 116, D24121, doi:10.1029/2011JD016387.

Hanna, E., Huybrechts, P., Steffen, K., Cappelen, J., Huff, R., Shuman, C., Irvine-Fynn, T., Wise, S., and Griffiths, M. 2008. Increased runoff from melt from the Greenland ice sheet: A response to global warming. Journal of Climate, 21, 331–341.

Hanna, E., McConnell, J., Das, S., Cappelen, J., and Stephens, A. 2006. Observed and modelled Greenland Ice Sheet snow accumulation, 1958–2003, and links with regional climate forcing. Journal of Climate, 19(3), 344–358, doi:10.1175/JCLI3615.1.

Hanna, E., Navarro, F. J., Pattyn, F., Domingues, C., Fettweis, X., Ivins, E., Nicholls, R. J., Ritz, C., Smith, B., Tulaczyk, S., Whitehouse, P., and Zwally, J. 2013. Ice-sheet mass balance and climate change. Nature, 498, 51–59.

Hanna, E., Mernild, S. H., Cappelen, J., and Steffen, K. 2012. Recent warming in Greenland in a long-term instrumental (1881–2012) climatic context. Part 1: Evaluation of surface air temperature records. Environmental Research Letters, 7, 045404, doi:10.1088/1748-9326/7/4/045404.

Haper, J., Humphrey, N., Pfeffer, W. T., Brown, J. and Fettweis, X. 2012. Greenland ice-sheet contribution to sae-level rise buffered by meltwater storage in firn. Nature, 22117–22124.

Hasholt, B., Mikkelsen, A. B., Nielsen, H. M, and Larsen, M. A. D. 2013. Observations of Runoff and Sediment and Dissolved Loads from the Greenland Ice Sheet at Kangerlussuaq, West Greenland, 2007 to 2010. Zeitschrift für Geomorphologie, 57(2), 3–27, doi:10.1127/0372-8854/2012/S-00121.

Hewitt, I. 2013. Seasonal changes in ice sheet motion due to melt water lubrication. Earth Plant. Sci. Lett., 371–372, 16–25.

Hiemstra, C. A., Liston, G. E., and Reiners, W. A. 2006. Observing, modelling, and validating snow redistribution by wind in a Wyoming upper treeline landscape. Ecol. Model. 197, 35–51, doi: 10.1016/j.ecolmodel.2006.03.005.

Hurrell, J. W. 1995. Decadal trends in the North Atlantic Oscillation: regional temperatures and precipitation. Science, 269, 676–679. doi:10.1126/science.269.5224.676.

Hurrell, J. W. and van Loon, H. 1997. Decadal variations in climate associated with the North Atlantic oscillation, Climate Change, 36, 301–326.

Kaplan, A., Cane, M. A., Kushnir, Y. and Clement, A. C. 1998. Analyses of global sea surface temperatures 1856–1991. Journal of Geophysical Research, 103, 18575–18589.

Kobayashi, S., Ota, Y., Harada, Y., Ebita, A., Moriya, M., Onoda, H., Onogi, K., Kamahori, H., Kobayashi, C., Endo, H., Miyaoka, K., and Takahashi, K. 2015. The JRA-55 Reanalysis: General Specifications and Basic Characteristics, J. Meteorol. Soc. Jpn., 93, 5–48, doi:10.2151/jmsj.2015-001.

Kohler, T. J., Zarsky, J. D., Yde, J. C., Lamarche-Gagnon, G., Hawkings, J. R., Tedstone, A. J., Wadham, J. L., Box, J. E., Beaton, A., and Stibal, M., 2017. Carbon dating reveals seasonal shifts in the source of sediments exported from the Greenland Ice Sheet. Geophys. Res. Lett., 44(12), 6209–6217.

Koziol, C., Arnold, N., Pope, A., and Colgan, W., 2017. Quantifying supraglacial meltwater pathways in the Paakitsoq region, West Greenland. J. Glaciol., 63(239), 464–476.

Langen, P. L., Mottram, R. H., Christensen, J. H., Boberg, F., Rodehacke, C. B., Stendel, M., van As, D., Ahlstrøm, A. P., Mortensen, J., Rysgaard, S., Petersen, D., Svendsen, K. H., Algeirsdottir, G. A., and Cappelen, J. 2015. Quantifying Energy and Mass Fluxes Controlling Godthåbsfjord Freshwater Input in a 5-km Simulation (1991–2012). Journal of Climate, 28, 3694–3713, doi:10.1175/JCLI-D-14-00271.1.

Lenaerts, J. T. M., Le Bars, D., van Kampenhout, L., Vizcaino, M., Enderlin, E. M., and van den Broeke, M. R. 2015. Representing Greenland ice sheet freshwater fluxes in climate models. Geophys. Res. Lett., 42, 6373–6381, doi:10.1002/2015GL064738.

Levinsen, J. F., Forsberg, R., Sørensen, L. S., and Khan, S. A. 2015. Essential Climate Variables for the Ice Sheets from Space and Airborne measurements. Danmarks Tekniske Universitet (DTU) PhD Thesis, Kgs. Lyngby, pp. 1–232.

Lewis, S. M., and Smith, L. C. 2009. Hydrological drainage of the Greenland ice sheet. Hydrol. Processes, 23, 2004–2011, doi:10.1002/hyp.7343.

Liston, G. E. 1995. Local advection of momentum, heat, and moisture during the melt of patchy snow covers. J. Appl.Meteorol., 34, 1705–1715, doi:10.1175/1520-0450-34.7.1705.

Liston, G. E. and Elder, K. 2006a. A distributed snow-evolution modeling system (SnowModel). J. Hydrometeorol., 7, 1259–1276, doi:10.1175/JHM548.1.

Liston, G. E. and Elder, K. 2006b. A meteorological distribution system for high-resolution terrestrial modeling (MicroMet). J. Hydrometeorol., 7, 217–234, doi:10.1175/JHM486.1.

Liston, G. E., Haehnel, R. B., Sturm, M., Hiemstra, C. A., Berezovskaya, S., and Tabler, R. D. 2007. Simulating complex snow distributions in windy environments using SnowTran-3D. J. Glaciol., 53, 241–256.

Liston, G. E. and Hiemstra, C. A. 2011. The changing cryosphere: pan-Arctic snow trends (1979–2009). J. Clim., 24, 5691–5712.

Liston, G. E. and Mernild, S. H. 2012. Greenland freshwater runoff. Part I: a runoff routing model for glaciated and non-glaciated landscapes (HydroFlow). J. Clim., 25(17), 5997–6014.

Liston, G. E. and Sturm, M. 1998. A snow-transport model for complex terrain. J. Glaciol., 44, 498–516.

Liston, G. E. and Sturm, M. 2002.Winter precipitation patterns in Arctic Alaska determined from a blowing-snow model and snow depth observations. J. Hydrometeorol., 3, 646–659.

Liston, G. E., Winther, J.-G., Bruland, O., Elvehøy, H., and Sand, K. 1999. Below surface ice melt on the coastal Antarctic ice sheet. J. Glaciol., 45, 273–285.

Machguth, H., MacFerrin, M., van as, D., Box, J., Charalampidis, C., Colgan, W., Fausto, R. S., Meijer, H. A. J., Mosley-Yhompson, E., and van de Wal, R. S. W. 2016. Greenland meltwater storage in firn limited by near-surface ice formation. Nature Climate Change, 6(4), 390–393, doi.org/10.1038/nclimate2899.

Mernild, S. H. 2016. Water balance from mountain glacier scale to ice sheet scale - With focus on Mittivakkat Gletscher, Southeast Greenland, and the Greenland Ice Sheet. Doctoral thesis. Faculty of Science, University of Copenhagen, Copenhagen, pp. 419.

Mernild, S. H., B. Hasholt and G. E. Liston 2006b. Water flow through Mittivakkat Glacier, Ammassalik Island, SE Greenland. Geografisk Tidsskrift-Danish Journal of Geography, 106(1), 25–43.

Mernild, S. H., Hanna, E., McConnell, J. R., Sigl, M., Beckerman, A. P., Yde, J. C., Cappelen, J., and Steffen, K. 2015. Greenland precipitation trends in a long-term instrumental climate context (1890–2012): Evaluation of coastal and ice core records. International Journal of Climatology, 35, 303–320, doi:10.1002/joc.3986.

Mernild, S. H. and Liston, G. E. 2010. The influence of air temperature inversion on snow melt and glacier surface mass-balance simulations, SW Ammassalik Island, SE Greenland. Journal of Applied Meteorology and Climate, 49(1), 47–67.

Mernild, S. H. and Liston, G. E. 2012. Greenland freshwater runoff. Part II: distribution and trends, 1960–2010. J. Clim., 25(17), 6015–6035.

Mernild, S. H., Liston, G. E., Hasholt, B., and Knudsen, N. T. 2006a. Snow distribution and melt modeling for Mittivakkat Glacier, Ammassalik Island, SE Greenland. Journal of Hydrometeorology, 7, 808–824.

Mernild, S. H., and Liston, G. E., and Hiemstra, C. A. 2014. Northern hemisphere glaciers and ice caps surface mass balance and contribution to sea-level rise. J. Clim., 27(15), 6051–6073, doi:10.1175/JCLI-D-13-00669.1.

Mernild, S. H., Liston, G. E., Hiemstra, C. A. and Christensen, J. H. 2010. Greenland Ice Sheet surface mass-balance modeling in a 131 year perspective 1950–2080. Journal of Hydrometeorology, 11(1), 3–25, doi.org/10.1175/2009JHM1140.1.

Mernild, S. H., Liston, G. E., Hiemstra, C. A., and Steffen, K. 2008. Surface Melt Area and Water Balance Modeling on the Greenland Ice Sheet 1995–2005. Journal of Hydrometeorology, 9(6), 1191–1211, doi.org/10.1175/2008JHM957.1.

Mernild, S. H., Liston, G. E., van As, D., Hasholt, B., and Yde, J. C. 2018. High-resolution ice sheet surface mass-balance and spatiotemporal runoff simulations: Kangerlussuaq, West Greenland. Arctic, Antarctic, and Alpine Research, , doi.org/10.1080/15230430.2017.1415856.

Mernild, S. H., Mote, T., and Liston, G. E. 2011. Greenland Ice Sheet surface melt extent and trends, 1960–2010. Journal of Glaciology, 57(204), 621–628.

Mernild, S. H., Liston, G. E., Hiemstra, C. A., Wilson, R. 2017. The Andes Cordillera. Part III: Glacier Surface Mass Balance and Contribution to Sea Level Rise (1979–2014). International Journal of Climatology, 37(7), 3154–3174, doi: 10.1002/joc.4907.

Metcalfe, J. R., Ishida, S., and Goodison, B. E. 1994. A corrected precipitation archive for the Northwest Territories of Canada, http://www.usask.ca/geography/MAGS/Data/Public_Data/precip_corr/pcpncor_e.htm.

Nghiem, S. V., Hall, D. K., Mote, T. L., Tedesco, M., Albert, M. R., Keegann, K., Shuman, C. A., DiGirolamo, N. E., and Neumann, G. 2012. The extreme melt across the Greenland ice sheet in 2012. *Geophysical Research Letters*, 39, L20502.

Nick, F. M., Vieli, A., Howat, I. M., and Joughin, I. R. 2009. Large-scale changes in Greenland outlet glacier dynamics triggered at the terminus. Nature Geoscience, 2(2), 110–114, doi:10.1038/ngeo394.

Noël, B., van de Berg, W. L., Lhermitte, S., Wouters; B., Machguth, H., Howat, I., Citterio, M., Moholdt, G., Lenaerts, J. T. M., and van den Broeke, M. R. 2017. A tipping point in refreezing accelerates mass loss of Greenland’s glaciers and ice caps. Nature Communications, 8, 1–8, doi:10.1038/ncomms14730.

Noël, B. van de Berg, W. J., Machguth, H., Lhermitte, S., Howat, I., Fettweis, X., and van den Broeke, M. R. 2016. A daily 1 km resolution data set of down scaled Greenland ice sheet surface mass balance (1958–2015). The Cryosphere, 10, 2361–2377, doi :10.5194/tc-10-2361-2016.

Overland, J. E., Francis, J., Hanna, E. and Wang, M. 2012. The recent shift in early summer arctic atmospheric circulation. Geophysical Research Letters, 39, L19804.

Preisendorfer, R.W. 1998. Principal Component Analysis in Meteorology and Oceanography. In: Mobley, C.D. (Ed.) Elsevier, Amsterdam, p. 452.

Rahmstorf, S., and Coauthors. 2005. Thermohaline circulation hysteresis: A model intercomparison. Geophys. Res. Lett., 32, L23605, doi:10.1029/2005GL023655.

Rasmussen, R., Baker, B., Kochendorfer, J., Meyers, T., Landolt, S., Fischer, A. P., Black, J., Theriault, J. M., Kucera, p., Gochis, D., Smith, C., Nitu, R., Hall, M., Ikeda, K., and Gutmann, E. 2012. How well are we measuring snow? The NOAA/FAA/NCAR Winter Precipitation Test Bed. BAMS, 811–829.

Rignot, E. and Mouginot, J. 2012. Ice flow in Greenland for the International Polar Year 2008–2009. Geophysical Research Letters, 39, L11501, doi:10.1029/2012GL051634.

Rignot, E., Velicogna, I., van den Broeke, M. R., Monaghan, A., and Lenaerts, J. 2011. Acceleration of the contribution of the Greenland and Antarctic ice sheets to sea level rise. Geophysical Research Letters, 38, L05503.

Roberts, M.J. 2005. Jökulhlaups: a reassessment of floodwater flow through glaciers. *Rev. Geophys.*, 43(1), RG1002, doi:10.1029/2003RG000147.

Rogers, A. N., Bromwich, D. H., Sinclair, E. N. and Cullather, R. I., 2001. The atmospheric hydrological cycle over the Arctic basins from reanalysis. Part II: Inter-annual variability. Journal of Climate, 14, 2414–2429.

Selmes, N., Murray, T., and James, T. D. 2011. Fast draining lakes on the Greenland ice sheet. Geophys Res. Lett., 38(15), doi:10.1029/2011GL047872.

Shepherd, A. et al. 2012. A Reconciled Estimate of Ice-Sheet Mass Balance. Science, 338, 1183–1189.

Sparnocchia S, Pinardi N, and Demirov E. 2003. Multivariate empirical orthogonal function analysis of the upper thermocline structure of the Mediterranean Sea from observations and model simulations. Ann. Geophys, 21, 167–187.

Sugden, D.E., Clapperton, C. M, and Knight, P. G.1985. A jökulhlaup near Søndre Strømfjord, West Greenland, and some effects on the ice-sheet margin. Journal of Glaciology, 31(109), 366–368.

Steger, C. R., Reijmer, C. H., van den Broeke, M. R., Wever, N., Forster, R. R., Koenig, L. S., Kuipers Munneke, P., Lehning, M., Lhermitte, S., Ligtenberg, S. R. M., Miège, C. and Noël, B. P. Y. 2017. Firn Meltwater Retention on the Greenland Ice Sheet: A Model Comparison. Front. Earth Sci. 5:3. doi: 10.3389/feart.2017.00003.

Steffen, K. 1995. Surface energy exchange at the equilibrium line on the Greenland ice sheet during onset of melt. Annals of Glaciology, 21, 13–18.

Straneo, F., Curry,R. G., Sutherland, D. A., Hamilton, G. S., Cenedese, C., Våge, K., and Sterns, L. A. 2011. Impact of fjord dynamics and glacial runoff on the circulation near Helheim Glacier. Nat.Geosci., 4, 322–327, doi:10.1038/ngeo1109.

Tedesco, M., Willis, I. C., Hoffman, M. J., Banwell, A. F., Alexander, P., and Arnold, N. S. 2013. Ice dynamic response to two modes of surface lake drainage on the Greenland ice sheet. Environ. Res. Lett., 8(3), 34007, doi:10.1088/1748-9326/8/3/034007.

Tedesco, M., Box, J. E., Cappelen, J., Fettweis, X., Mote. T., van de Wal, R. S. W., Smeets, C. J. P. P., and Wahr, J. 2014. Greenland Ice Sheet. In Jeffries, M. O., Richter-Menge, J. A., and Overland, J. E. (eds.). Arctic Report Card 2014.

Tedesco, M., Box, J. E., Cappelen, J., Fausto, R. S., Fettweis, X., Mote, T., Smeets C. J. P. P., van As, D., Velicogna, I., van de Wal, R. S. W. and Wahr, J. 2016. Greenland Ice Sheet. In Richter-Menge, J. A., Overland, J. E., and Mathis, J. T. (eds.). Arctic Card Report 2016.

Uppala, S. M., Kållberg, P. W., Simmons, A. J., Andrae, U., Da Costa Bechtold, V., Fiorino, M., Gibson, J.K., Haseler, J., Hernandez, A., Kelly, G. A., Li, X., Onogi, K., Saarinen, S., Sokka, N., Allan, R. P., Anderson, E., Arpe, K., Balmaseda, M. A., Beljaars, A. C. M., Van De Berg, L., Bidlot, J., Bormann, N., Caires, S., Chevallier, F., Dethof, A., Dragosavac, M., Fisher, M., Fuentes, M., Hagemann, S., Hólm, E., Hoskins, B. J., Isaksen, L., Janssen, P. A. E. M., Jenne, R., Mcnally, A. P., Mahfouf, J.-F., Morcrette, J.-J., Rayner, N. A., Saunders, R.W., Simon, P., Sterl, A., Trenbreth, K. E., Untch, A., Vasiljevic, D., Viterbo, P., and Woollen, J.: The ERA-40 re-analysis, Q. J. Roy. Meteor. Soc., 131, 2961–3012, doi:10.1256/qj.04.176, 2005.

van Angelen, J. H., Lenaerts, J. T. M., van den Broeke, J. T. M., Fettweis, X., van Meijgaard, E. 2013. Rapid loss of firn pore space accelerates 21 century Greenland mass loss. Geophysical Research Letter, 40, 2109–2113.

van As., D, Box, J. E., and Fausto, R. S., 2016: Challenges of Quantifying Meltwater Retention in Snow and Firn: An Expert Elicitation. Frontiers in Earth Science, 4(101), 1–5.

van As, D. Hasholt, B., Ahlstrøm, A. P., Box, J. E., Cappelen, J., Colgan, W., Fausto, R. S., Mernild, S. H., Mikkelsen, A .B., Noël, B. P.Y., Petersen, D., and Van den Broeke, M. R. 2018. The longest observationally-constrained record of Greenland ice sheet meltwater discharge (1949–2016). Accepted, Arctic, Antarctic, and Alpine Research (Special Issue).

van den Broeke, M. R., Enderlin, E. M., Howat, I. M., Munneke, P.K., Noël, B. P., Y., van de Berg, W. J., van Meijgaard, E., and Wouters, B. 2016. On the recent contribution of the Greenland ice sheet to sea level change. The Cryosphere, 10, 1933–1946, doi:10.5194/tc-10-1933-2016.

van den Broeke, M., Smeets, P., Ettema, J., and Munneke, P. K. 2008a. Surface radiation balance in the ablation zone of the west Greenland ice sheet, J. Geophys. Res., 113, D13105, doi:10.1029/2007/JD009283.

van den Broeke, M., Smeets, P., Ettema, J., van der Veen, C., van de Wal, R., and Oerlemans, J. 2008b. Partitioning of melt energy and meltwater fluxes in the ablation zone of the west Greenland ice sheet, The Cryosphere, 2, 179–189, doi:10.5194/tc-2-179-2008.

van de Wal, R. S. W., Greuell, W., van den Broeke, M. R., Reijmer, C. H., and Oerlemans, J. 2005. Surface mass-balance observations and automatic weather station data along a transect near Kangerlussuaq, West Greenland, Ann. Glaciol., 42, 311–316.

van de Wal, R. S. W., Boot, W., van den Broeke, M., Smeets, C. J. P. P., Reijmer, C. H., Donker, J. J. A., and Oerlemans, J. 2008. Large and rapid melt-induced velocity changes in the ablation zone of the Greenland ice sheet. Science, 321, 111–113.

van der Veen, C. J. 2007. Fracture propagation as a means of rapidly transferring surface meltwater to the base of glaciers. Geophys. Res. Lett., 34, L01501.

Weijer, W.,M. E. Maltrud, M. W. Hecht, H. A. Dijkstra, and M. A. Kliphuis, 2012. Response of the Atlantic Ocean circulation to Greenland Ice Sheet melting in a strongly-eddying ocean model. Geophys. Res. Lett., 39, L09606, doi:10.1029/2012GL051611.

Wilton, D. J., Jowett, A., Hanna, E., Bigg, G. R., van den Broeke, M. R., Fettweis, X., and Huybrechts, P., 2017. High resolution (1 km) positive degree-day modelling of Greenland ice sheet surface mass balance, 1870-2012 using reanalysis data. Journal of Glaciology, 63(237), 176–193.

Vizcaino, M., Lipscomb, W. H., Sacks, W. J., van Angelen, J. H, Wouters, B., and van den Broeke, M. R. 2013. Greenland Surface Mass Balance as Simulated by the Community Earth System Model. Part I: Model Evaluation and 1850‑2005 Results. Journal of Climate, 26, 7793–7812, doi.10.1175/JCLI-D-12-00615.1.

Yang, D., Ishida, S., Goodison, B. E., and Gunter, T. 1999. Bias correction of daily precipitation measurements for Greenland. J. Geophys. Res. 104(D6), 6171–6181, doi:10.1029/1998JD200110.

Zwally, H. J., Abdalati, W., Herring, T., Larson, K., Saba, J., and Steffen, K. 2002. Surface melt-induced acceleration of Greenland ice-sheet flow. Science, 297, 218–222.

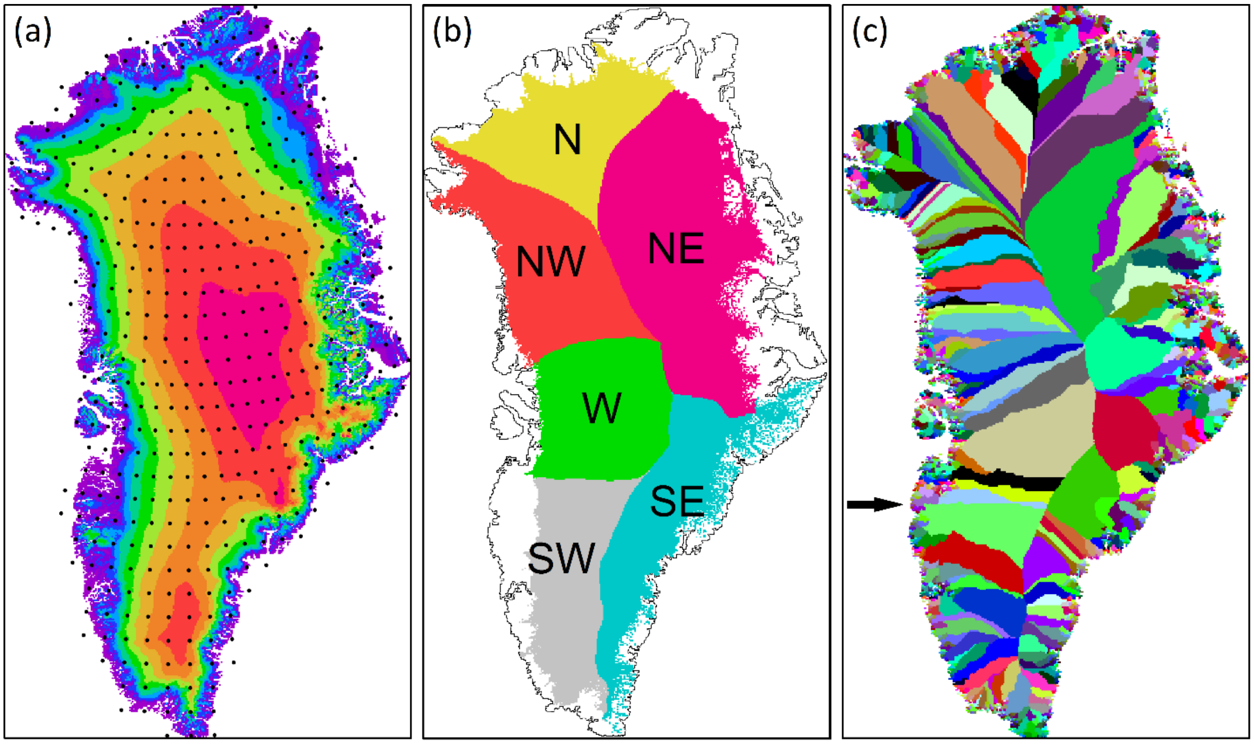

Figure 1: (a) Greenland simulation domain with topography (500-m contour interval) and locations of ERA-I atmospheric forcing grid points used in the model simulations (black dots; to improve clarity only every other grid point was plotted in x and y, i.e., 25 % of the grid points used are shown); (b) the major regional division of the GrIS following Rignot et al. (unpublished); and (c) HydroFlow simulated individual Greenland drainage catchments (*n* = 3,272; represented by multiple colors). The approximate location of the Kangerlussuaq catchment is shown with a black arrow from where the SnowModel evaluations were conducted.

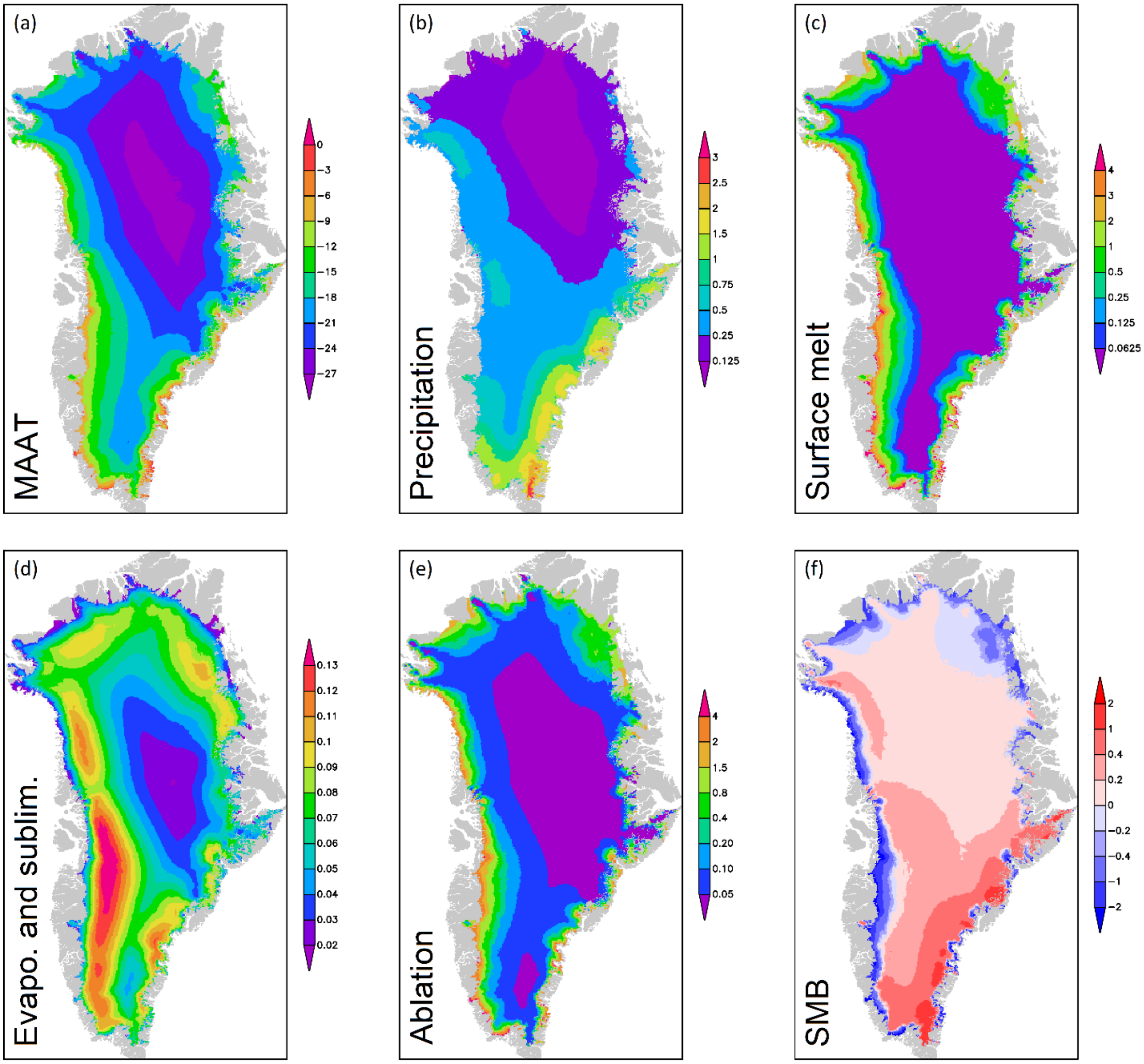

Figure 2: SnowModel ERA-I simulated 35-year mean spatial GrIS surface (1979–2014): (a) MAAT (°C); (b) precipitation (m w.e.); (c) surface melt (snow and ice melt) (m w.e.); (d) evaporation and sublimation (m w.e.); (e) ablation (m w.e.); and (f) SMB (m w.e.).

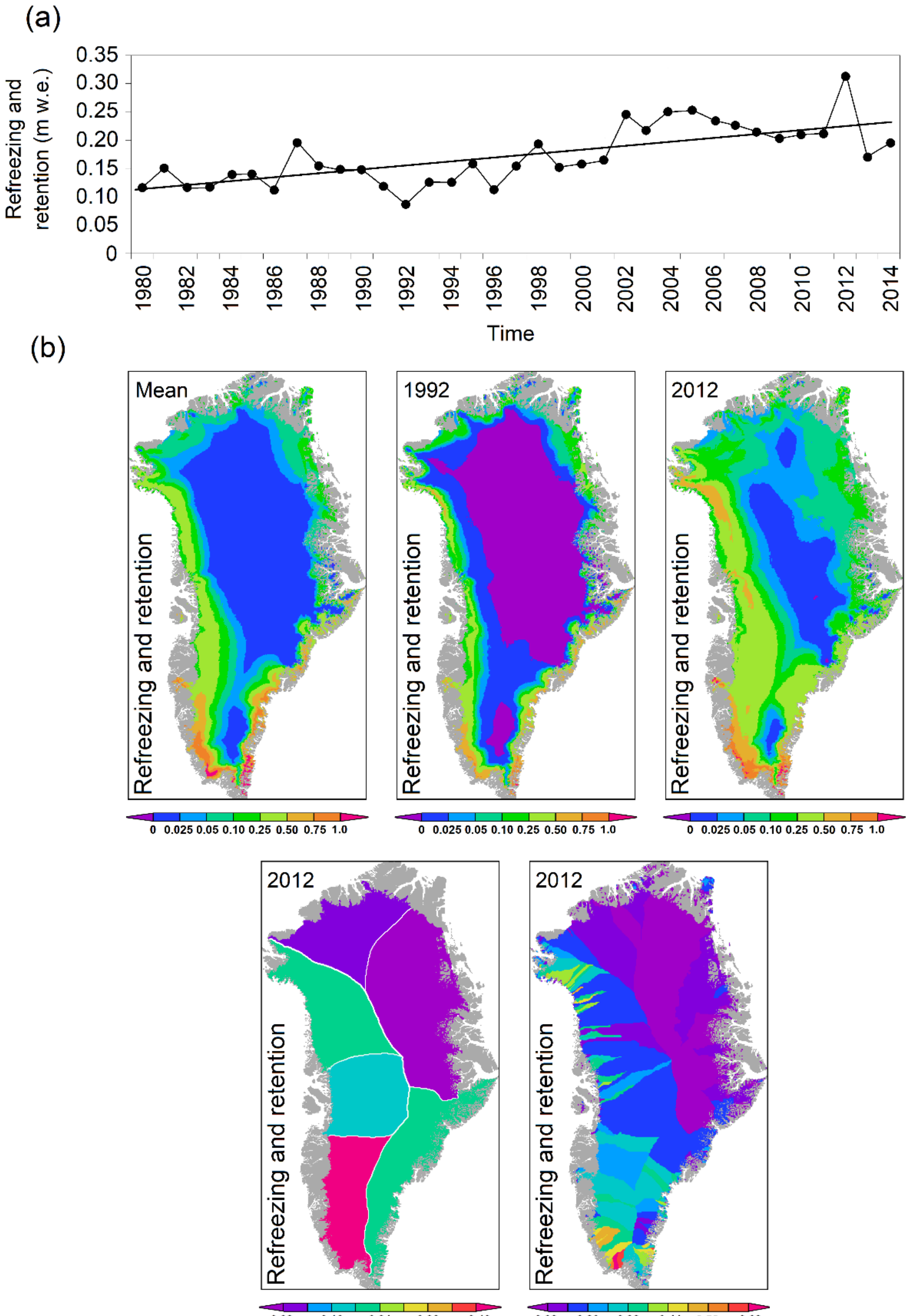

Figure 3: (a) SnowModel ERA-I simulated time series of GrIS mean annual refreezing and retention (1979–2014) (m w.e.); and (b) spatial 35-year mean GrIS refreezing and retention and annual values (m w.e) for 1992 and 2012 (upper row), together with the 2012-division into regions (lower row left) and catchments (lower row right).

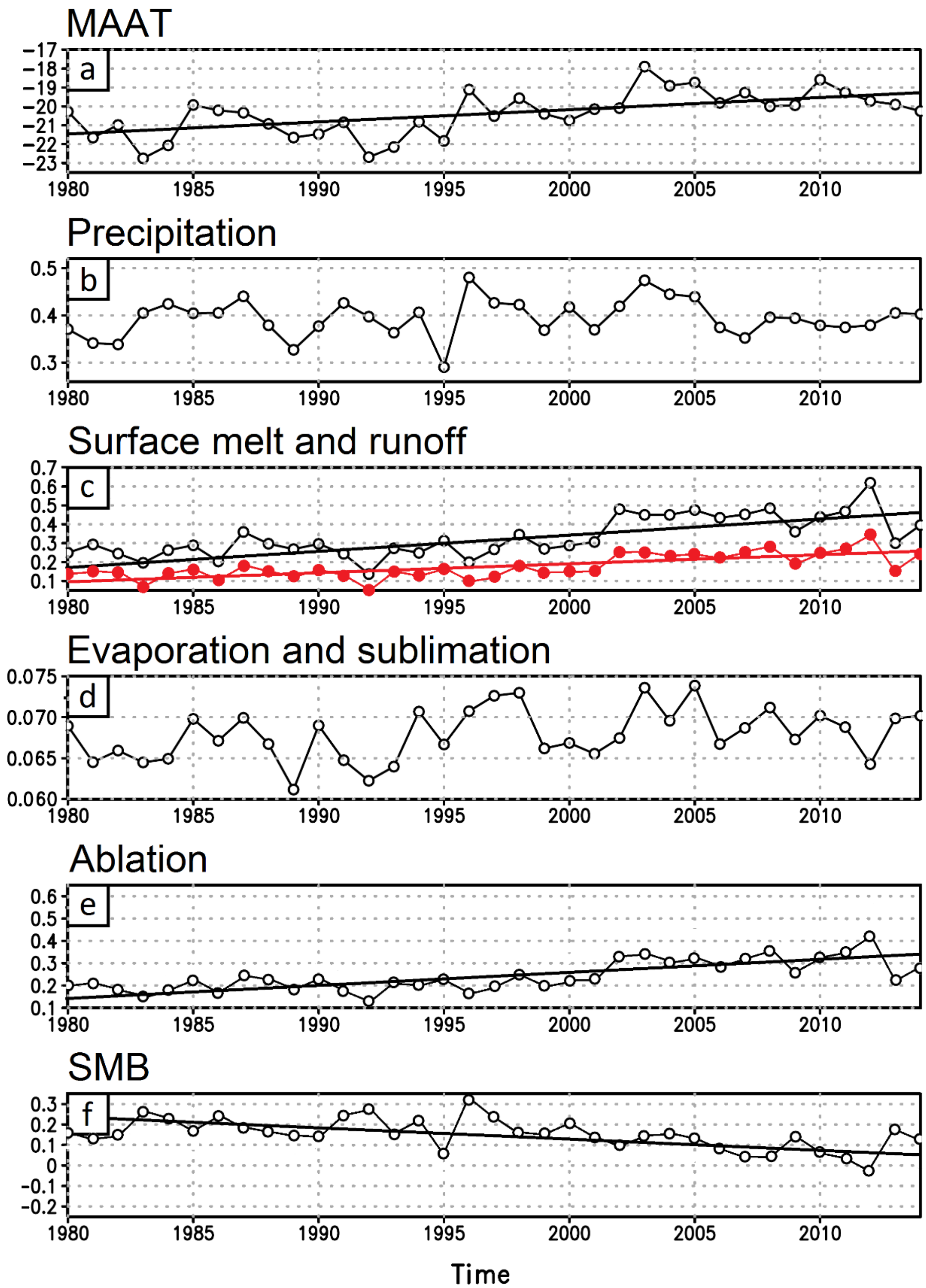

Figure 4: SnowModel ERA-I simulated time series of GrIS annual mean (1979–2014): (a) MAAT (°C); (b) precipitation (m w.e.); (c) surface melt (snow and ice melt) and runoff (red time series) (m w.e.); (d) evaporation and sublimation (m w.e.); (e) ablation (m w.e.); and (f) SMB (m w.e.). Only significant linear trends are shown.

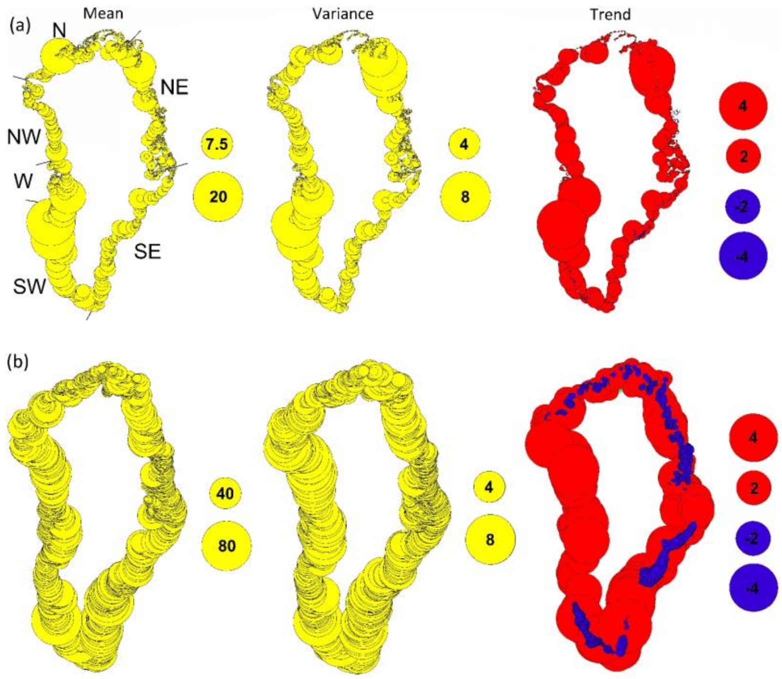

Figure 5: SnowModel ERA-I simulated 35-year spatial Greenland catchment runoff (1979–2014): (a) mean runoff ($\times 10^9$ m^3) (the locations of the major regions SW, W, NW, etc., are illustrated), runoff variance (here illustrated as one standard deviation; $\times 10^9$ m^3), and decadal runoff trends (linear; $\times 10^9$ m^3 $decade^{-1}$) (catchments with increasing runoff trends are shown with red and decreasing trends with blue colors); and (b) mean specific runoff (L s^{-1} km^{-2}), specific runoff variance (L s^{-1} km^{-2}), and specific runoff trends (linear; L s^{-1} km^{-2} $decade^{-1}$).

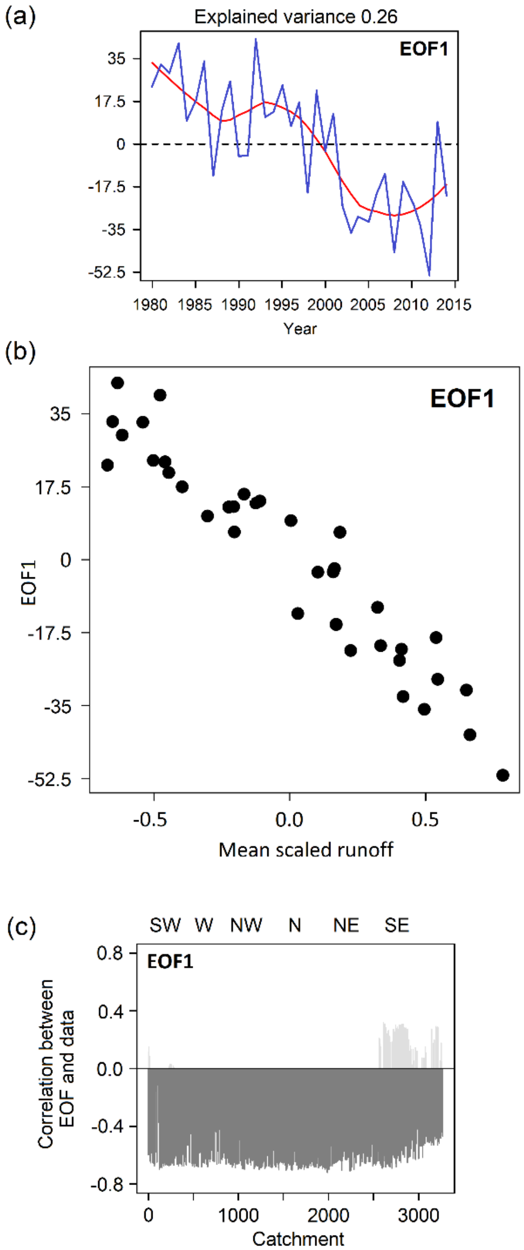

Figure 6: (a) SnowModel ERA-I simulated runoff time series (1979–2014) of the empirical orthogonal functions (black curve) and 5-year running mean smoothing line (red curve) of EOF1 (significant); (b) EOF1 cross correlation relationships with mean annual scaled runoff from Greenland; and (c) Eigenvector correlation values for each simulated catchment (1 to 3,272) for EOF1. From left to right on the lower x-axis the catchments follows the clockwise path from the southern tip of Greenland (Southwest Greenland, Catchment 1) to the northern part (N section) and back to the southern tip (Southeast Greenland, Catchment 3,272). The location of the major regions: SW, W, NW, etc., are shown on the upper x-axis.

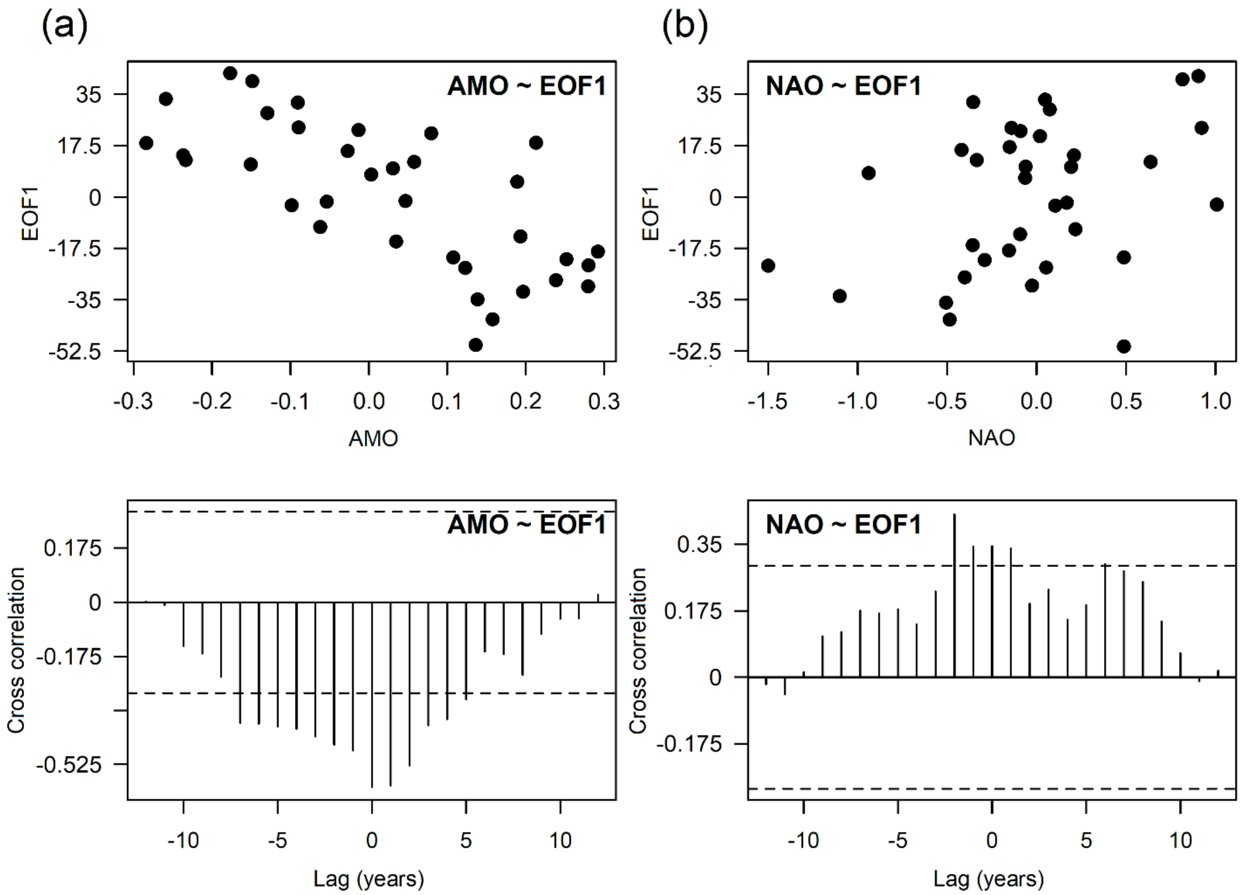

Figure 7: EOF1 cross correlation relationships between simulated Greenland runoff: (a) AMO and (b) NAO. The horizontal dashed lines on each of the column charts indicate the significance (95% confidence).

Table 1: Regional breakdown of GrIS surface mean annual conditions (units are in Gt) and trends (linear; Gt decade^{-1}): precipitation (P) (including rain and snow), surface melt, evaporation (E) and sublimation (Su), runoff (R), ablation, refreezing and retention (rain and surface melt minus runoff), and surface mass-balance (SMB) for GrIS and for each of the six regions both from 1979–2014 (35 years) and 2005–2014 (10 years). Specifically for rain the %-value of total precipitation is shown. Trends are shown in paragraphs for the GrIS column. Significant trends ($p < 0.05$) are highlighted in bold.

	N (229,075 km^2)	NE (454,900 km^2)	SE (250,425 km^2)	SW (213,550 km^2)	W (231,150 km^2)	NW (267,075 km^2)	GrIS (1,646,175 km^2)
1979–2014							
P	31.1 ± 5.4	68.4 ± 10.6	242.6 ± 39.1	142.3 ± 23.3	85.4 ± 13.5	84.2 ± 13.9	653.9 ± 66.4 (9.0)
P (rain)	0.4 ± 0.2 (1 %)	0.4 ± 0.2 (<1 %)	4.2 ± 1.8 (2 %)	6.6 ± 2.8 (5 %)	1.7 ± 0.8 (2 %)	2.2 ± 1.1 (3 %)	15.3 ± 5.4 (2 %) (**3.0**)
P (snow)	30.7 ± 5.3	68.0 ± 10.5	238.5 ± 38.7	135.7 ± 22.7	83.7 ± 13.2	82.0 ± 13.5	638.6 ± 65.0 (6.0)
Surface melt	57.2 ± 24.1	72.2 ± 33.8	101.0 ± 27.1	155.2 ± 48.4	67.4 ± 24.0	89.8 ± 33.2	542.9 ± 175.3 (**121.7**)
E + Su	15.7 ± 0.9	25.3 ± 1.6	16.8 ± 0.8	20.3 ± 1.7	16.4 ± 1.1	17.7 ± 0.9	112.2 ± 5.2 (1.8)
R	34.5 ± 15.7	43.3 ± 21.8	47.8 ± 14.5	77.7 ± 28.9	37.0 ± 13.4	48.4 ± 19.4	288.7 ± 104.3 (**73.4**)
Ablation (E + Su + R)	50.2 ± 15.6	68.5 ± 21.8	64.6 ± 14.9	98.1 ± 29.2	54.4 ± 13.9	66.0 ± 19.8	400.9 ± 106.2 (**75.2**)
Refreezing and retention	23.1 ± 8.7 (40 %)	29.4 ± 12.5 (41 %)	57.5 ± 14.5 (57 %)	84.1 ± 23.2 (54 %)	32.1 ± 11.4 (46 %)	43.7 ± 14.9 (48 %)	269.9 ± 77.4 (49 %) (**51.3**)
SMB	-19.2 ± 17.9	-0.2 ± 23.3	178.1 ± 41.7	44.3 ± 39.2	32.1 ± 18.9	18.2 ± 24.4	253.4 ± 121.4 (**-66.2**)
2005–2014							
P	30.9 ± 5.1	71.0 ± 11.9	232.4 ± 25.2	138.5 ± 16.1	86.4 ± 8.6	85.3 ± 16.9	645.0 ± 39.0 (-5.1)
P (rain)	0.5 ± 0.3 (2 %)	0.4 ± 0.2 (<1 %)	5.2 ± 1.9 (2 %)	7.8 ± 2.3 (6 %)	2.0 ± 0.6 (2 %)	2.9 ± 1.3 (4 %)	18.7 ± 3.4 (3 %) (-2.8)
P (snow)	30.4 ± 5.0	70.6 ± 11.9	227.1 ± 25.0	130.8 ± 15.7	84.4 ± 8.6	82.9 ± 16.4	626.3 ± 39.2 (-2.3)
Surface melt	75.9 ± 26.9	101.7 ± 34.5	129.7 ± 16.3	202.4 ± 39.2	89.3 ± 19.7	124.6 ± 26.8	713.4 ± 138.6 (-79.7)
E + Su	15.7 ± 1.0	25.9 ± 1.1	17.3 ± 0.9	20.7 ± 1.5	16.7 ± 0.8	17.8 ± 0.9	114.1 ± 4.3 (-3.8)
R	46.6 ± 17.3	61.7 ± 21.4	63.3 ± 10.0	106.6 ± 25.0	49.1 ± 10.5	68.7 ± 15.5	395.4 ± 82.7 (-26.0)
Ablation (E + Su + R)	62.3 ± 17.0	87.6 ± 21.2	80.6 ± 9.7	127.3 ± 23.9	65.9 ± 10.2	86.5 ± 15.6	510.0 ± 81.7 (-17.9)
Refreezing and retention	29.7 ± 10.0 (39 %)	40.5 ± 13.6 (40 %)	66.4 ± 8.7 (51 %)	95.8 ± 18.5 (47 %)	40.2 ± 9.9 (45 %)	55.9 ± 13.0 (45 %)	318.0 ± 62.8 (45 %) (-64.6)
SMB	-31.4 ± 18.7	-16.5 ± 22.0	151.8 ± 32.0	11.3 ± 34.5	20.6 ± 12.6	-0.7 ± 24.3	135.5 ± 98.2 (16.6)

Table 2: Regional breakdown of GrIS specific runoff (L s^{-1} km^{-2}) for GrIS and each of the six individual sections both from 1979–2014 and 2005–2014.

	N	NE	SE	SW	W	NW	GrIS
1979–2014	4.8	3.0	6.0	11.5	5.1	5.7	5.6
2005–2014	6.5	4.3	8.0	15.8	6.7	8.2	7.6

Supplementary Material

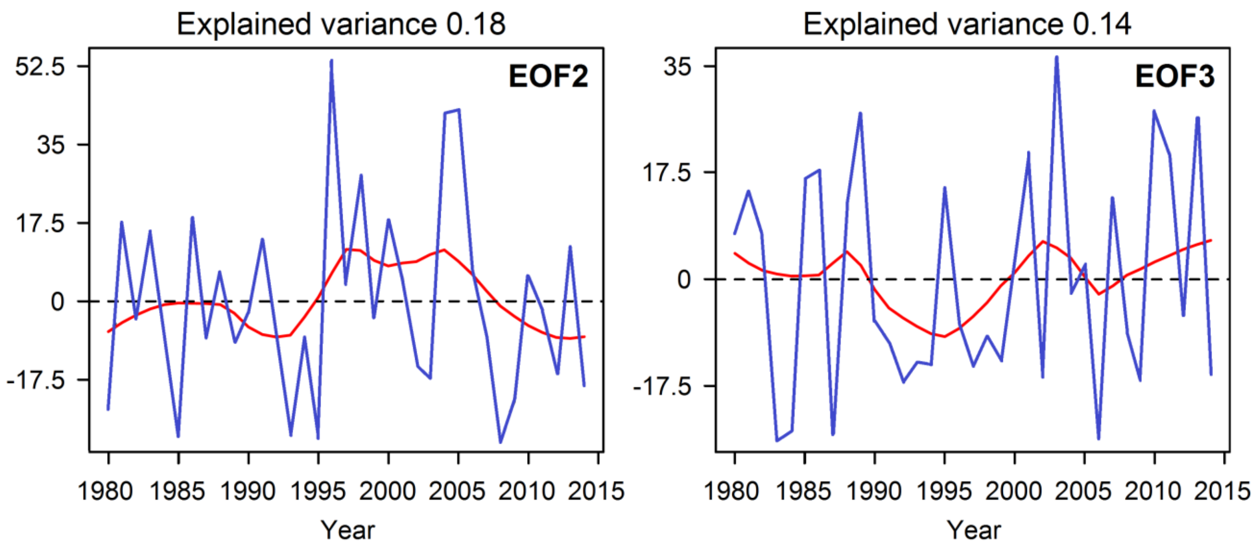

Figure S1: SnowModel ERA-I simulated runoff time series (1979–2014) of the empirical orthogonal functions (black curve) and 5-year running mean smoothing line (red curve) of EOF2 and EOF3. The explained variance is shown for each EOF. Both EOF2 and EOF were insignificant.

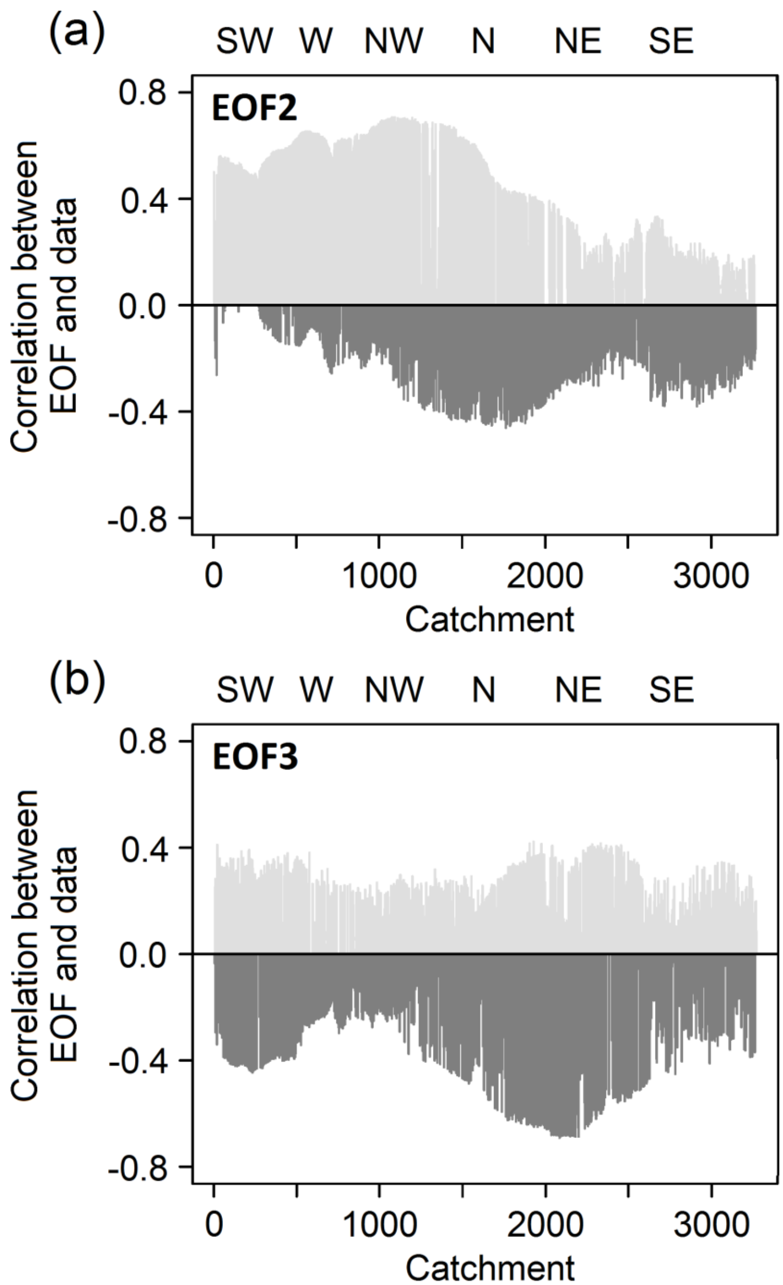

Figure S2: Eigenvector correlation values for each simulated catchment (1 to 3,272) for: (a) EOF2 and (b) EOF3. From left to right on the lower x-axis the catchments follows the clockwise path from the southern tip of Greenland (Southwest Greenland, Catchment 1) to the northern part (N section) and back to the southern tip (Southeast Greenland, Catchment 3,272). The location of the major regions: SW, W, NW, etc., are shown on the upper x-axis.